# Transcriptional antitermination integrates the expression of loci of diverse phage origin in the chimeric *Bartonella* Gene Transfer Agent BaGTA

Aleksandr Korotaev[1], Quirin Niggli[1], Valeria Congedi[1] and Christoph Dehio[1,*]

[1] Biozentrum, University of Basel, Spitalstrasse 41, CH-4056 Basel, Switzerland

* To whom correspondence should be addressed at christoph.dehio@unibas.ch

**Abstract**

Gene Transfer Agents (GTAs) are mobile genetic elements derived from bacteriophages that mediate genome-wide horizontal gene transfer (HGT) in diverse groups of prokaryotes. BaGTA, encoded by all the pathogens of the genus *Bartonella*, is a chimeric GTA that evolved by the domestication of two phages. The run-off-replication module ROR of one phage is integrated with the capsid production, DNA packaging and lysis machinery Bgt of a second phage. Restricted to a self-sacrificing subset of the bacterial population, the position-specific DNA amplification and packaging of a genomic plasticity region enriched for genes involved in host interaction and adaptation selectively enhances the HGT frequency of these pathogenicity genes. This feature of BaGTA is considered a key innovation underlying the evolutionary success of *Bartonella*. Little is known, however, about the mechanism mediating the coordinated expression of the *ror* and *bgt* loci. Here, we established the regulatory hierarchy, with *ror* acting upstream of the capsid gene cluster *bgtA-K*. BrrG, encoded by the *ror* locus, controls the transcription of the *bgtA-K* operon by functioning as a processive antiterminator. This study provides the first insights into the mechanism controlling the coordinated expression of the two BaGTA modules of divergent phage origin. Beyond BaGTA, we propose that antitermination is a broadly relevant mechanism for controlling HGT by GTAs of the Alphaproteobacteria.

## Introduction

Timed and tightly controlled gene expression is crucial in bacterial cells. A variety of mechanisms to control transcription are known, comprising both positive and negative regulators (reviewed in Turnbough, 2019). One of the mechanisms of negative regulation involves transcription attenuation at termination sites (reviewed in Santangelo and Artsimovitch, 2011). The regulation of transcription attenuation is achieved by a diverse class of antiterminators which counteract the attenuation (Santangelo and Artsimovitch, 2011). Antiterminators fall into two categories and can either act specifically at a single, defined terminator site or convert RNA polymerase into a termination-resistant complex that is generally resistant to multiple termination sites over a longer distance (Santangelo and Artsimovitch, 2011; reviewed in Goodson and Winkler, 2018). In the latter case, such antiterminators are referred to as processive antiterminators. Well-known examples of processive antiterminators are Q and N of bacteriophage lambda which control progression of the infection cycle (Goodson and Winkler, 2018).

Peculiar examples of phage evolution are Gene Transfer Agents (GTAs) (reviewed in Québatte and Dehio, 2019; Banks and Tung, 2024; Craske et al., 2024). GTAs are mobile genetic elements, which emerged from defective temperate bacteriophages. GTAs encode bacteriophage-like particles and in contrast to phages transfer unspecific pieces of host bacterial DNA. Despite their phage origin, GTAs are not self-transmitting because the DNA packaging capacity of a GTA particle is too small to package the entire gene cluster encoding it. Therefore, GTAs are transferred vertically (Banks and Tung, 2024; Craske et al., 2024; Kogay et al., 2022; Lang et al., 2012). GTAs are found both in bacteria and archaea, and are one of the non-canonical mechanisms of horizontal gene transfer (HGT) (Arnold et al., 2022).

Bacterial pathogens of the genus *Bartonella* encode a chimeric GTA known as BaGTA (Québatte and Dehio, 2019; Berglund et al., 2009; Guy et al., 2013). BaGTA encodes the gene clusters *bgtA-K,* responsible for the synthesis and assembly of GTA particles, *bgtL-R*, with orphan functions, and *bgtS-V*, involved in putative host cell lysis (Fig. 1A). DNA packaging in GTA particles is coupled to a process of site-specific DNA amplification mediated by the *ror* locus located in between the *bgtL-R* and *bgtS-V* gene clusters. This locus, emerging from a

different phage domestication event, includes an origin of run-off replication (ROR) and the associated *brr* gene cluster *(brrA-G)* (Berglund et al., 2009; Guy et al., 2013; Québatte et al., 2017; Tamarit et al., 2018) (Fig. 1A). The *bgtA-K* and *ror* loci are located within a high plasticity zone of the genome that is prone to DNA integrations and is highly enriched for genes encoding virulence properties involved in host interaction and adaptation (Berglund et al., 2009; Guy et al., 2013). This specific genome architecture leads to ROR-driven amplification and packaging of these pathogenicity genes, resulting in elevated transfer rates to other *Bartonella* bacteria compared to housekeeping genes encoded more distantly to the ROR origin (Québatte et al., 2017). This process is considered to provide the recombination substrates for the duplication and evolutionary diversification of genes encoding the type IV secretion systems (T4SSs) and cognate effector proteins which collectively represent a key innovation associated with the adaptive radiation of these pathogens to diverse mammalian hosts (Guy et al., 2013; Engel et al., 2011). Additionally, it is also considered to facilitate the fast evolution of surface-located autotransporters serving in host interaction and adaptation, such as the recombination-driven antigenic variation of the CFA autotransporter (Siewert et al., 2022). Thus, BaGTA is a crucial factor for the fitness and adaptability of pathogens in the *Bartonella* genus (Québatte and Dehio, 2019). However, little is known about how the expression of the *bgt* and *brr* loci derived from separate phages is regulated in a coordinated manner.

In this study, we elucidated the regulatory hierarchy between the *bgtA-K* and *ror* loci, resolving the mechanism of gene expression control. We discovered that BaGTA operates under a strict regulatory framework, with a protein encoded by the *ror* locus and controlling the expression of the *bgtA-K* capsid-production locus. Specifically, our research revealed that in absence of BaGTA activation, transcription of the *bgtA-K* locus is attenuated by a putative terminator site. Upon BaGTA activation by a yet unknown process, the *ror* locus-encoded BrrG overcomes this transcription attenuation of the *bgtA-K* locus by acting as a processive antiterminator. Furthermore, we propose that antitermination is a common mechanism of GTA regulation in the Alphaproteobacteria. Collectively, these findings offer significant insights into the regulation of BaGTA-mediated gene transfer in pathogens of the genus *Bartonella* and

84 suggest a broader impact of processive antitermination as a regulatory principle in related
85 GTAs.

## Results

### BrrG shows structural similarity to the P21 phage-encoded Q21 antiterminator and is essential for GTA transfer and expression of capsid components

Previously, we identified by multiplexed transposon sequencing the genes of BaGTA encoding both for donor transfer and recipient uptake functions (Québatte et al., 2017). However, many of the identified genes had only hypothetical or no functional sequence-based annotation, leaving their contribution to BaGTA function unclear. To address this knowledge gap, we employed the protein structure prediction tool AlphaFold2 to model unannotated proteins of BaGTA genes and searched the Protein Data Bank (PDB) database for similar structures. We discovered that the *brrG* gene (Fig. 1A), which is located in the *ror* locus, encodes a protein with structural similarity to the antiterminator Q21 of the lambdoid bacteriophage P21 (Fig. 1B). Q21 and its counterpart Q from phage λ (Qλ) function as processive antiterminators involved in bypassing intrinsic terminators (Guo et al., 1991; Grayhack and Roberts, 1982). This enables uninterrupted expression of the late genes, which encode capsid morphogenesis and lysis cassettes. Therefore, we hypothesized that, similar to Q21 and Qλ, BrrG represents a putative antiterminator controlling gene expression within the BaGTA regulatory network.

To test this hypothesis, we assessed the effect of *brrG* overexpression on the transcription of the *bgtA-K* locus that encodes components of the capsid synthesis and assembly machinery as essential components of BaGTA production. We utilized the previously established reporter strain *bgtC-gfp* that contains a promoter-less *gfpmut2* inserted in the *bgtA-K* locus in the intergenic region between *bgtC* and *bgtB* (Québatte et al., 2017) (Fig. 1A). This transcriptional reporter enabled us to monitor *bgtA-K* expression over time using flow cytometry (Fig. 1C, upper panel). We observed that plasmid-based overproduction of BrrG increased the fraction of GFP fluorescent bacteria up to 75%, compared to about 15% at native BrrG expression (Fig. 1D), thus massively expanding the fraction of cells expressing the *bgtA-K* locus. To test whether this increase is followed by GTA production and elevated DNA transfer, we performed the GTA transfer assay. For that, we cocultivated donor and recipient cells carrying different resistance markers followed by plating on selective media to enumerate double-resistant bacteria as a read-out for the frequency of GTA-mediated gene transfer (Fig. 1C, lower panel). We observed

115 that - while the proportion of cells expressing the BaGTA locus increased as a result of BrrG
116 overproduction, GTA transfer rates remained similar to native BrrG expression (Fig. 1E). In
117 contrast, deleting *brrG* led to a significant decrease in the proportion of fluorescent bacteria (Fig.
118 1F) and caused DNA transfer rates to drop at least 100-fold compared to those observed at
119 native BrrG expression (Fig. 1G). Together, these findings indicate that BrrG plays a crucial role
120 in regulating BaGTA. It is capable of activating the expression of capsid components in a large
121 part of the population that is initially GTA inactive. However, overproduction of BrrG is not
122 sufficient to increase the rate of DNA transfer, indicating that it acts in concert with other
123 regulators controling other crucial steps of this complex process.

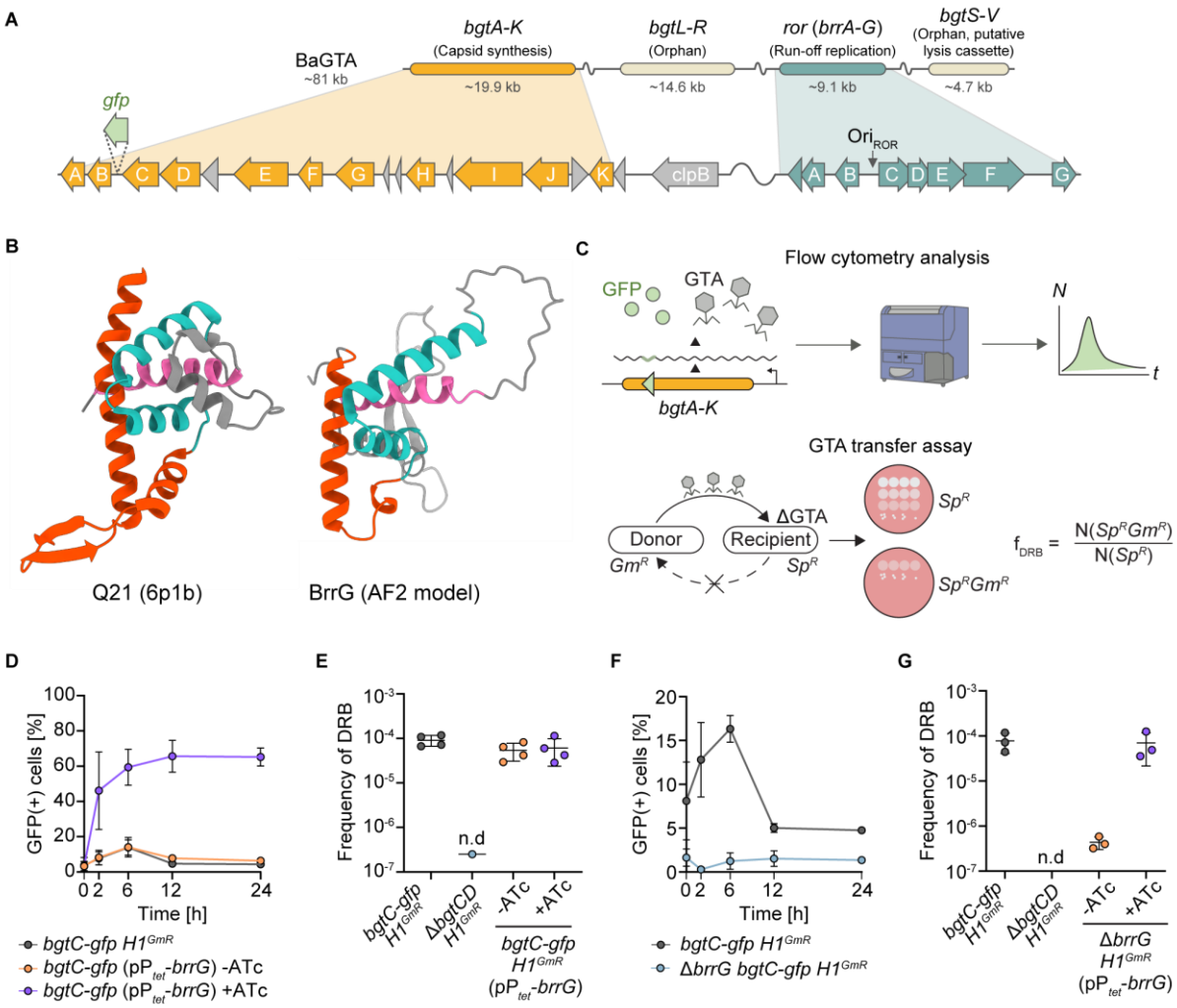


**Figure 1. BrrG encodes a putative antiterminator essential for *bgtA-K* expression and BaGTA-mediated gene transfer. (A)** Schematic representation of the BaGTA locus. Upper

part: Structure and size of the *bgtA-K* and *ror* gene clusters. Lower part: Close-up of the *bgtA-K* locus encoding capsid and packaging functions and of the *ror* locus, encoding the run-off-replication origin $ori_{ROR}$ and the associated *brrA-G* gene cluster. For the reporter strain *bgtC-gfp* and its derivatives used in D-G, the insertion site of the transcriptional *gfp* reporter within the *bgtA-K* locus is indicated. **(B)** Comparison of the structure of Q21 antiterminator (6p1b) of phage P21 and Alphafold2 model of BrrG (A0A0R4J952). Similar structural features are presented in identical colour. **(C)** Schematic presentation of (i) the flow cytometry assay to monitor expression of the *bgtA-K* locus using the *bgtC-gfp* transcriptional reporter strain (upper panel) and (ii) the assay to monitor GTA transfer via transfer of $Gm^R$ from the GTA-positive donor strain to the *ΔbgtCD* $Sp^R$ GTA-negative (ΔGTA) recipient strain resulting in $Sp^RGm^R$ bacteria and formula to calculate the frequency of double resistant bacteria ($f_{DRB}$) as a proxy for GTA transfer. **(D)** BrrG overproduction increases the bacterial population expressing *bgtA-K*. BrrG expression was induced in strain *bgtC-gfp* ($pP_{tet}$-*brrG*) with anhydrotetracycline (aTc). Strain *bgtC-gfp* $H1^{GmR}$ (*bgtC-gfp BH01490::Himar1*$^{GmR}$) displaying wild-type properties served as a positive control. **(E)** BrrG overproduction does not enhance GTA transfer. Strain *bgtC-gfp* $H1^{GmR}$ displaying wild-type properties and the GTA-negative mutant Δ*bgtCD* $H1^{GmR}$ (*ΔbgtCD BHRS00695::Himar1*$^{GmR}$) served as a positive and negative control, respectively. **(F)** Deletion of *brrG* (Δ*brrG bgtC-gfp* $H1^{GmR}$ [*ΔbrrG BH01490::Himar1*$^{GmR}$]) results in reduced expression of the *bgtA-K* locus. **(G)** Overproduction of BrrG in a Δ*brrG* mutant background restores GTA transfer frequency to the wild-type level. BrrG expression was induced in strain Δ*brrG* $H1^{GmR}$ ($pP_{tet}$-*brrG*) with aTc. **(D-G)** The time-course experiments were started with the incubation of CBA agar-grown bacteria in M199 medium supplemented with 10% FCS. 25 ng/ml aTc was added where indicated to induce expression by the $P_{tet}$ promoter. The experiments were performed in biological triplicates (D, F, G) or quadruplicates (E), error bars indicate SD.

124 **BrrG binds in proximity to the $P_{bgtA-K}$ promoter located upstream of to the putative *bgtA-K***
125 **operon**

126 In lambdoid phages, both Q21 and Qλ are DNA-binding proteins that recognize a motif located
127 in the promoter region of the late operon, which encodes lysis cassettes and proteins required
128 for capsid morphogenesis (Guo et al., 1991; Grayhack and Roberts, 1982; Yin et al., 2019; Shi
129 et al., 2019; Yin et al., 2022). Considering the structural similarity between BrrG and Q21, we
130 hypothesized that BrrG may be functionally conserved and thus able to directly bind to DNA at
131 the yet unidentified promoter of the *bgtA-K* locus. To test this, we performed chromatin
132 immunoprecipitation of epitope-tagged BrrG followed by DNA sequencing. We found that BrrG
133 binds to DNA, with a single binding site located in the intergenic region far upstream of the *bgtK*

134 gene representing the first conserved gene of the *bgtA-K* locus (Fig. 2A, Suppl. Figure 2) (Guy
135 et al., 2013; Tamarit et al., 2018). Given this remote upstream location of the BrrG binding site,
136 we wondered whether the promoter elements might also be located nearby. First, we tested
137 whether the 999 bp fragment spanning the region upstream of *bgtK* until the end of *clpB* could
138 drive expression of a fused promoter-less *dsRed* gene using flow cytometry as readout (Fig. 2A,
139 plasmid p*Pf3-dsRed*). Strikingly, this fragment did not only demonstrate promoter activity but
140 also displayed at the population level a temporal control resembling closely the expression
141 pattern of the chromosomal transcriptional reporter strain *bgtC-gfp H1*$^{GmR}$ with a characteristic
142 peak in the size of expressing population at the 6 h time-point of the 24 h expression kinetic
143 (Fig. 2B). This finding suggests that the *bgtA-K* locus is organized as a transcriptional unit
144 (operon) that is driven by a promoter localizing to the 999 bp fragment upstream of *bgtK*, which
145 we thus named $P_{bgtA\text{-}K}$ (Fig. 2A).

146 Next, to narrow down the location of $P_{bgtA\text{-}K}$, we split the 999 bp fragment into three
147 partially overlapping fragments and tested them with the same approach using a *gfpmut2*-based
148 promoter-probe plasmid (plasmids p*sF1*, p*sF2* and p*sF3,* Fig. 2A). We observed that the most
149 upstream fragment spanning nucleotides 594-999 was able to drive broad expression of
150 *gfpmut2* at population level (plasmid p*sF3* in Figure 2C). The fraction of fluorescent bacteria
151 was substantially higher compared to the chromosomal transcriptional reporter strain *bgtC-gfp*,
152 expanding beyond 40% at each time-point (Fig. 2C, Suppl. Figure 3). Importantly, the lack of
153 temporal regulation as seen by the chromosomal transcriptional reporter strain *bgtC-gfp* and
154 likewise the 999 bp fragment in plasmid Pf3 (compare Figs. 2B and 2C) suggests that absence
155 of downstream control elements located in the more proximal region spanning nucleotides 1-
156 593 converted $P_{bgtA\text{-}K}$ into a constitutive state. To map $P_{bgtA\text{-}K}$ based on conserved elements (-10
157 and -35 boxes) we aligned corresponding sequences from a selection of *Bartonella* species
158 covering the genomic diversity of this genus. By this comparative approach, we identified a
159 highly conserved sequence motive (TTGACA-$N_{17}$-TATCAT) that shows almost full identity to the
160 canonical sigma-70 promoter sequence of *E. coli* (-35 box: 100%, -10 box: >80%, Fig. 2D)
161 (Campbell et al., 2002; Murakami et al., 2002). This suggests that $P_{bgtA\text{-}K}$ functions as a minimal

162 promoter of the *bgtA-K* locus. Interestingly, the BrrG binding region coincides with $P_{bgtA-K}$,
163 suggesting that BrrG controls transcription either by direct binding to $P_{bgtA-K}$ or in the vicinity of it.
164 Taken together, we identified $P_{bgtA-K}$ as a strong constitutive promoter located far
165 upstream of the *bgtA-K* locus, driving its expression as a transcriptional unit along with more
166 proximal elements required for controlling temporal expression at the population level.
167 Additionally, we found that the putative antiterminator BrrG, similar to Q21 and Qλ, is a DNA-
168 binding protein that directly binds to $P_{bgtA-K}$ and likely controls *bgtA-K* operon expression at
169 population level.

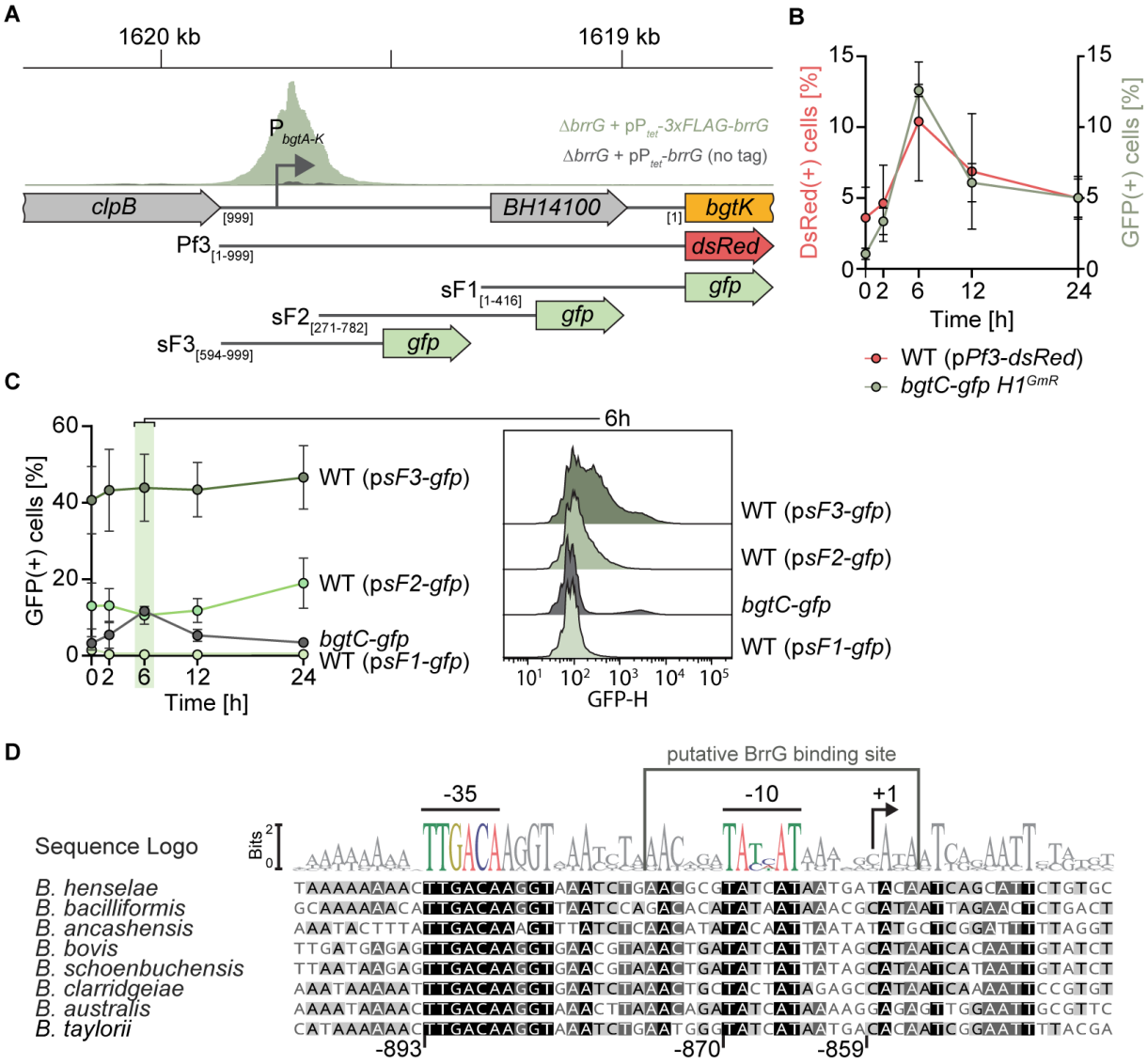


**Figure 2. BrrG binds in proximity to the $P_{bgtA-K}$ promoter located upstream of the putative *bgtA-K* operon. (A)** Location of the $P_{bgtA-K}$ promoter and of the BrrG binding site identified by

ChIP-Seq (gray histogram). Δ*brrG* + p$P_{tet}$-*brrG* (no tag) is shown in dark grey; Δ*brrG* + p$P_{tet}$-*3x-FLAG-brrG* is shown in green. The fragments upstream of the *bgtA-K* locus were tested for promoter activity in promoter-probe plasmids as indicated. **(B)** The fusion of the 999 bp fragment spanning from the region between *bgtK* and *clpB* to *dsRed* (strain WT ($P_{Pf3}$-*dsRed*) displays a temporal transcriptional profile similar to the chromosomal transcription reporter for the *bgtA-K* locus (strain *bgtC-gfp H1*$^{GmR}$ [*bgtC-gfp BH01490::Himar1*$^{GmR}$]). **(C)** The $P_{bgtA-K}$ promoter is located far upstream of the *bgtA-K* locus. Left: Temporal transcriptional profiles controlled by fragments spanning nucleotide 1-416 (plasmid p*sF1*), nucleotides 271-782 (plasmid p*sF2*), or nucleotides 594-999 (plasmid p*sF3*) of the 999 bp fragment in Pf3. Right: Corresponding histograms of fluorescence distribution at the 6 h time-point. Strain *bgtC-gfp* displaying wild-type expression pattern of the *bgtA-K* locus was used as control. **(D)** DNA sequence alignment of the predicted promoter region and putative BrrG binding site within psF3 fragment with homologous sequences from various *Bartonella* species. The predicted -35 and -10 promoter elements and the inferred transcriptional start site (+1) are indicated. Numbers below indicate the location of the promoter elements relative to *bgtK*. (B, C) The time-course experiments were started with the incubation of CBA agar-grown bacteria in M199 medium supplemented with 10% FCS. The experiments were done in biological triplicates, error bars indicate SD.

170 **A long leader sequence attenuating expression is located downstream of the $P_{bgtA-K}$**
171 **promoter**

172 To confirm that the identified conserved sequence is the promoter and to hint at the function of
173 the long downstream sequence in transcription, we generated a panel of promoter-probe
174 plasmids harbouring truncations of the 999 bp fragment bearing promoter activity (p*F0-gfp* to
175 p*F6-gfp*) (Fig. 3A). We observed that the 29 bp fragment spanning the predicted $P_{bgtA-K}$
176 displayed fluorescence in the vast majority of cells, confirming the promoter prediction (F0
177 fragment, Fig. 3B). Similar promoter activities were recorded for the fragments F1 and F2 that
178 are extended by 27 bp or 133 bp towards the *bgtA-K* locus, respectively. A striking difference in
179 fluorescence distribution, with an almost complete loss of fluorescent bacteria, was observed for
180 the F3 fragment, which contains an additional 139 bp relative to F2 (Fig. 3B, Suppl. Figure 4).
181 Fragments F4-F6 with further downstream extensions also displayed pattern of low
182 fluorescence, while a bi-model distribution with low- and intermediate-expressing bacteria was
183 observed for fragments F4 and F6.

184 Because fragment F3 is the shortest fragment displaying reduced expression, we
185 hypothesized that a terminator could be present in the sequence extending the highly
186 fluorescent F2 fragment. Indeed, a putative L-shaped terminator with a free energy (ΔG) of -6
187 kcal/mol is predicted within the stretch of 139 bp of the F3 fragment, which might explain the
188 observed difference in expression levels (Fig. 3C). Altogether, these results demonstrate that
189 the minimal promoter enables uniform and constitutive expression of the BaGTA locus at
190 population level. The observed temporal regulation and heterogeneity of the gene cluster
191 expression appear to be provided by the stretch of 864 bp located downstream of the promoter
192 and upstream to *bgtK* as first gene of the *bgtA-G* locus. This stretch of DNA contains the
193 putative terminator and could harbour other terminators or additional regulatory elements.

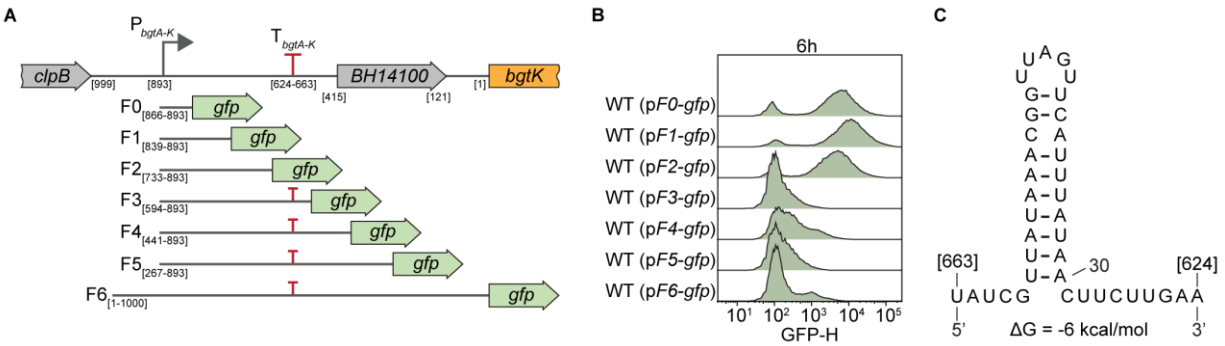


**Figure 3. A putative terminator is encoded in the long non-protein coding sequence downstream of the $P_{bgtA-K}$ promoter. (A)** Schematic representation of the 5'-part of the *bgtA-K* locus with the truncations tested with promoter-probe plasmids. Locations of the $P_{bgtA-K}$ promoter and the predicted terminator are shown. **(B)** Histograms of fluorescence distribution measured for the bacterial populations containing the promoter-probe plasmids with various truncations at 6 h. **(C)** Predicted secondary structure and free energy of the putative $T_{bgtA-K}$ terminator. Numbers in parentheses indicate the location of the terminator relative to *bgtK*. The time-course experiment was started with the incubation of CBA plate-grown bacteria in M199 medium supplemented with 10% FCS. Experiments were performed in biological triplicates.

194 **A -10-like element is required for expression of the *bgtA-K* locus**

195 In phage lambda, the process of Q-mediated antitermination relies on the engagement of Q into
196 the complex with RNA-polymerase (RNAP) and the conversion of the latter into a termination-
197 resistant form (Perdue and Roberts, 2011). This process begins with RNAP pausing at the -10-

198 like element, a six-nucleotide motif (NANNNT), located just downstream of the -10 promoter
199 element, which allows Q to engage with the transcription complex (Perdue and Roberts, 2011).
200 Therefore, we set out to determine whether a -10-like element is present in the vicinity of
201 the identified $P_{bgtA\text{-}K}$ minimal promoter. We examined the previously generated alignment and
202 identified a conserved NANNNT site located 5 bp downstream of the identified promoter $P_{bgtA\text{-}K}$
203 (Fig. 4A). As the conserved nucleotides A and T at positions +2 and +6 in phage lambda and
204 other phages are also conserved in this motif directly downstream of $P_{bgtA\text{-}K}$, we hypothesized
205 that this site could act as a -10-like element (Fig. 4A). To validate this hypothesis, we used the
206 promoter-probe plasmid containing the F6 fragment (Fig. 3A), and introduced two point
207 mutations, replacing the conserved A in position +2 to G and T in position +6 to C (p$F6_{(-10mut)}$-
208 *gfp*), respectively. Additionally, we introduced a second plasmid directing aTc-inducible BrrG
209 overproduction to test whether these mutations would affect the activity of the putative
210 antiterminator in the flow cytometry assay (Fig. 1C). In contrast to plasmid p*F6-gfp* encoding the
211 native -10-like element (Fig. 4B, left, -aTc), p$F6_{(-10mut)}$-*gfp* did not display the characteristic
212 kinetics of GFP-expression of wild-type bacteria with a peak at 6 h (Fig. 4B, right, -aTc, Suppl.
213 Figure 5). Moreover, neither did it display the massive expansion of the GFP-expressing
214 population upon BrrG overproduction (+aTc) (Fig. 4B, Suppl. Figure 5). Thus, the replacement
215 of two conserved nucleotides at the putative -10-like element completely abolished transcription
216 of the downstream *bgtA-K* locus under both native BrrG expression and BrrG overproduction
217 conditions. This suggests that the identified conserved site is a functional -10-like element
218 essential for the BrrG-mediated antitermination.

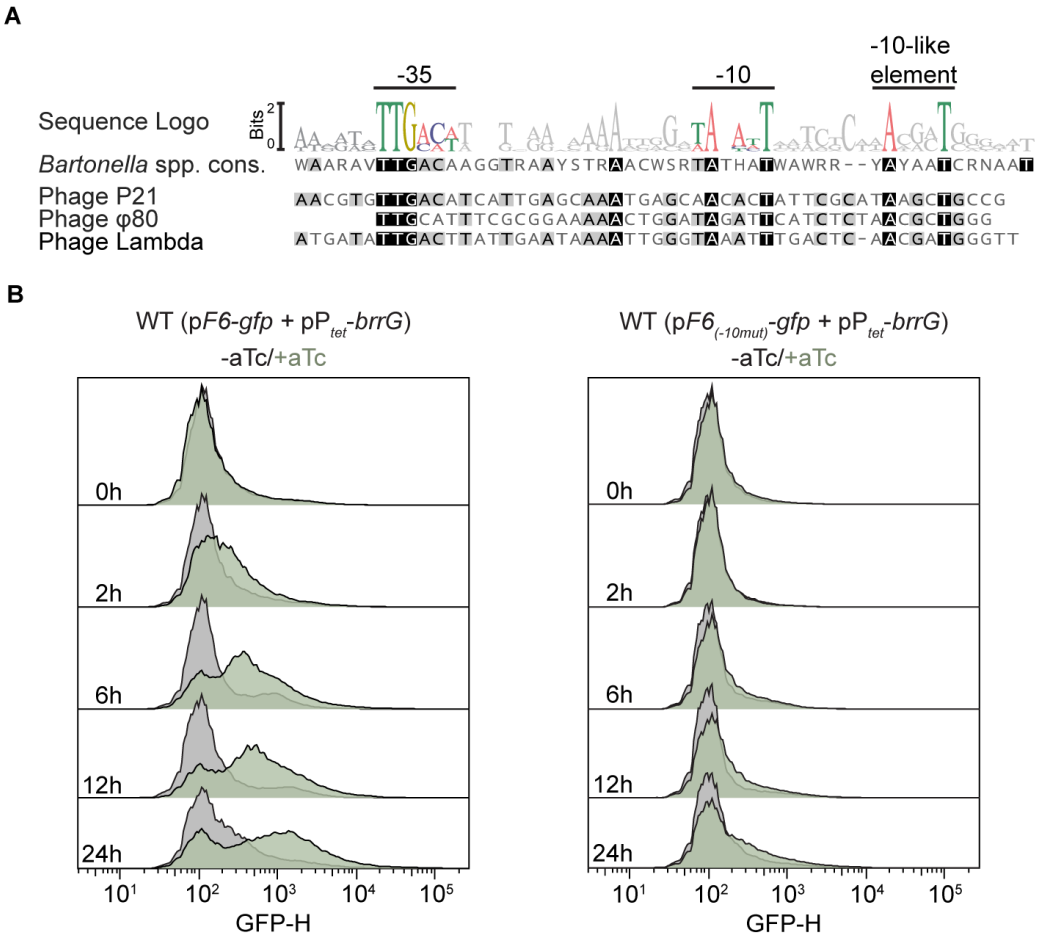


**Figure 4. The -10-like element downstream of the $P_{bgtA\text{-}K}$ promoter is crucial for the antitermination by BrrG. (A)** Alignment of *Bartonella* spp. consensus and lambdoid phage sequences (P21, phi80 and lambda) sequences containing $P_{bgtA\text{-}K}$ and the $P_{R'}$ promoters followed by the -10-like elements, respectively. Promoter -35 and -10 elements, as well as the -10-like elements are marked. **(B)** Histograms of fluorescence distribution for the bacterial populations containing the promoter-probe plasmid pF6 (compare to Fig. 3A) with the $P_{bgtA\text{-}K}$ promoter and the adjacent native -10-like element or its derivative, plasmid p*F6*$_{(-10mut)}$, carrying mutations in two conserved positions of the -10-like element. Plasmid p$P_{tet}$-*brrG* encodes an aTc-inducible *brrG* expression cassette. BrrG overproduction was induced by 25 ng/ml aTc. The time-course experiment was started with the incubation of CBA plate-grown bacteria in M199 medium supplemented with 10% FCS. Inducer aTc was added at time-point 0 h. Experiments were performed in biological triplicates.

**BrrG is a processive antiterminator allowing RNAP to bypass the termination site.**

We showed that BrrG shares structural features with the processive antiterminator Q21 and that its function is dependent on the -10-like element suggesting that BrrG belongs to the class of processive antiterminators. To validate this hypothesis, we tested the antitermination properties

223 of BrrG towards a synthetic terminator. For this, we used the artificially designed strong
224 terminator BBa_B1006 from the iGEM collection and placed it in between the F2 fragment (see
225 Fig. 3A), which contains the native $P_{bgtA\text{-}K}$ promoter and downstream -10-like element, but not
226 the native terminator and the *gfp* reporter gene (Fig. 5A). The plasmid p*F2-gfp* containing the
227 terminator-less fragment F2 drives GFP-expression in a large part of the bacterial population at
228 both BrrG native expression and overproduction conditions (Figs. 3B and 5B). In contrast, the
229 derivative p$F2\text{-}T_{BBa_1006}$-*gfp* containing in addition the artificial terminator showed a strongly
230 reduced population expression of GFP, but a marked increase in GFP-expressing bacteria upon
231 BrrG overproduction (Fig. 5B, right panel, Suppl. Figure 6). Together, these findings
232 demonstrate that the presence of BrrG allows the RNAP to bypass both the native termination
233 site, as well as an unrelated synthetic terminator, indicating that BrrG is indeed a processive
234 antiterminator.

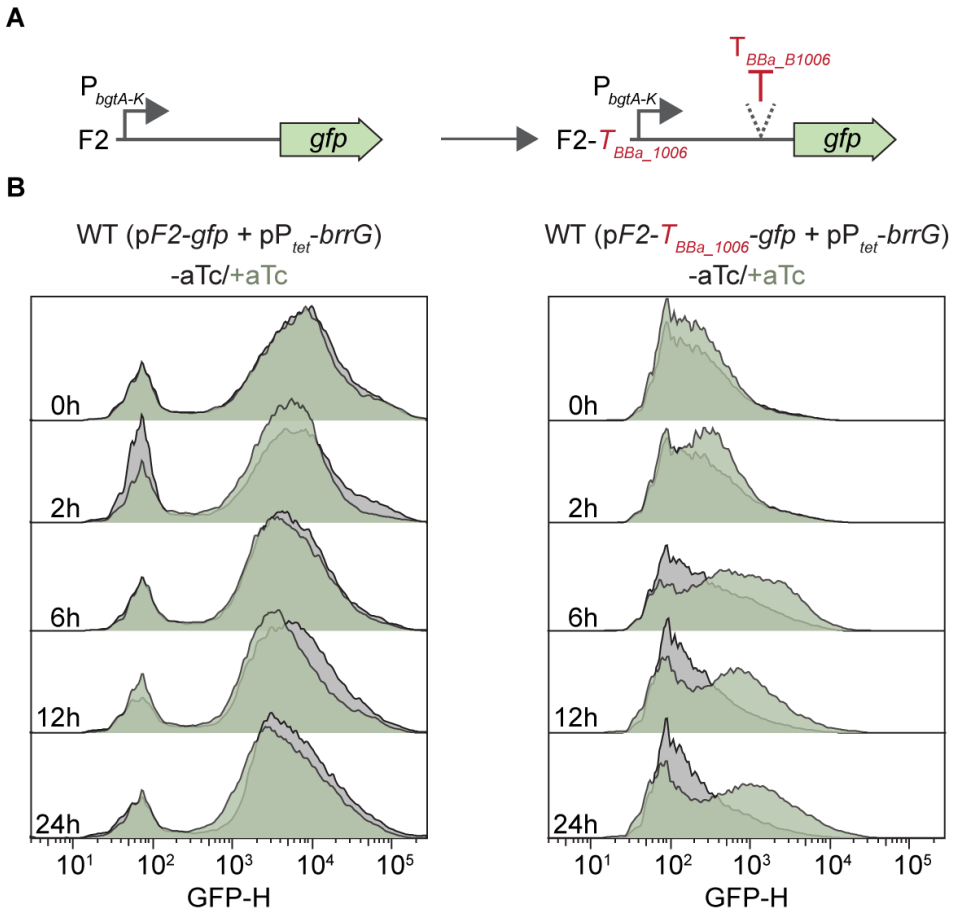


**Figure 5. Antiterminator BrrG allows RNA polymerase to bypass an engineered**

**termination site. (A)** Schematic representation of the experimental setup. Plasmid p*F2-*$T_{BBa_1006}$*-gfp* carries the insertion of the artificial strong terminator $T_{BBa_1006}$ in between the terminator-less promoter fragment F2 and *gfp* of plasmid pF2-*gfp.* **(B)** Histograms of fluorescence distribution for the bacterial populations containing the fragment F2, the fragment F2 with the terminator and the sequence with the mutated -10-like element (pF6$_{-10mut}$). Time of the measurements is indicated. Induction was done with 25 ng/ml aTc. Bacteria were cultivated in M199 medium supplemented with 10% FCS and aTc inducer at indicated concentrations. Experiments were performed in biological triplicates.

235

236 **Discussion**

237 Processive antitermination is an important mechanism of transcriptional control identified
238 both for bacteria and phages. In temperate phages processive antiterminators, i.e. phage
239 lambda N and Q-antiterminators, switch on expression of early and late genes, respectively, and
240 thus enable the progression of the infection cycle (Goodson and Winkler, 2018).

241 Given the ancestral relationship between GTAs and phages, this study investigates
242 whether transcription attenuation and antitermination are preserved in the chimeric BaGTA and
243 whether they play a role in the regulatory integration of two functional gene clusters of divergent
244 phage origin. We showed that the "late" capsid producing *bgtA-K* genes belong to a single
245 transcriptional unit derived from one phage, and that their expression is enabled by the
246 antiterminator BrrG, encoded within the *ror* locus, which originates from a second phage.
247 However, the question remains: Is BrrG a Q-like antiterminator, and does it function in a similar
248 manner?

249 The canonical Q-dependent regulatory circuit consists of several critical components: Q
250 antiterminator, the promoter $P_{R'}$, a termination site and a -10-like element (Perdue and Roberts,
251 2011; reviewed in Casjens and Hendrix, 2015). The first component is the Q antiterminator
252 which binds to DNA and engages into the complex with RNAP. The Q-RNAP complex is
253 termination-resistant and permits RNAP to bypass the termination signals in front of late genes
254 which results in the synthesis of the capsid components (Guo et al., 1991; Grayhack and
255 Roberts, 1982). In our study we showed that BrrG has structural similarity to the Q21
256 antiterminator of the P21 lambdoid phage. Moreover, BrrG is able to counteract transcription
257 attenuation imposed by an introduced artificial termination site. Additionally, we demonstrated
258 that BrrG binds in proximity to the $P_{bgtA\text{-}K}$ promoter and upregulates transcription of the *bgtA-K*
259 cluster – BaGTA's counterpart of the late gene cluster.

260 The second component of the canonical Q-dependent regulatory circuit is the promoter
261 $P_{R'}$ containing Q-binding site for interaction with Q and engagement with RNAP. In this study, we
262 demonstrated that the $P_{bgtA\text{-}K}$ promoter overlaps with the BrrG binding site. Given that the

263 promoter $P_{bgtA\text{-}K}$ is located 864 bp upstream from the first gene of the *bgtA-K* cassette and is
264 separated from the former by a gene BH14100, this raises the question of whether BH14100
265 belongs to the *bgtA-K* cluster and what functional role it may play. Previous studies have shown
266 that BH14100 is not conserved among *Bartonellae* and thus is likely not involved in the BaGTA
267 regulation or synthesis (Guy et al., 2013; Tamarit et al., 2018). In support of this, our previous
268 study using multiplexed transposon sequencing showed no effect of BH14100 disruption on
269 GTA transfer, indicating that BH14100 has either no or only a very modest effect on GTA
270 synthesis (Québatte et al., 2017).

271 The third component of the canonical Q-dependent regulatory circuit is the termination
272 site which attenuates expression of the late gene cluster. We showed that the putative
273 terminator $T_{bgtA\text{-}K}$ is located downstream of the $P_{bgtA\text{-}K}$ promoter and regulates expression of the
274 *bgtA-K* operon. Whereas the *bgtA-K* locus is only active in the GTA producing cells, deleting the
275 putative terminator $T_{bgtA\text{-}K}$ renders broad and constitutive expression of the *bgtA-K* locus which
276 suggests that the temporal regulation and heterogeneity in expression are granted by $T_{bgtA\text{-}K}$.

277 The fourth component of the canonical Q-dependent regulatory circuit is the -10-like
278 element located in proximity to the promoter $P_{R'}$ driving expression of late genes. This element
279 resembles the -10-element of the promoter and defines the sigma-dependent pausing of RNAP
280 which is crucial for the engagement of Q into the complex with RNAP (Perdue and Roberts,
281 2011). We found that expression of the *bgtA-K* locus is dependent on the conserved -10-like
282 element located downstream of the $P_{bgtA\text{-}K}$ promoter. Altogether, these data suggest that BrrG is
283 an antiterminator found in BaGTA and involved in regulating expression of the *bgtA-K* cluster.
284 Based on these lines of evidence we propose BrrG as Q-like processive antiterminator.

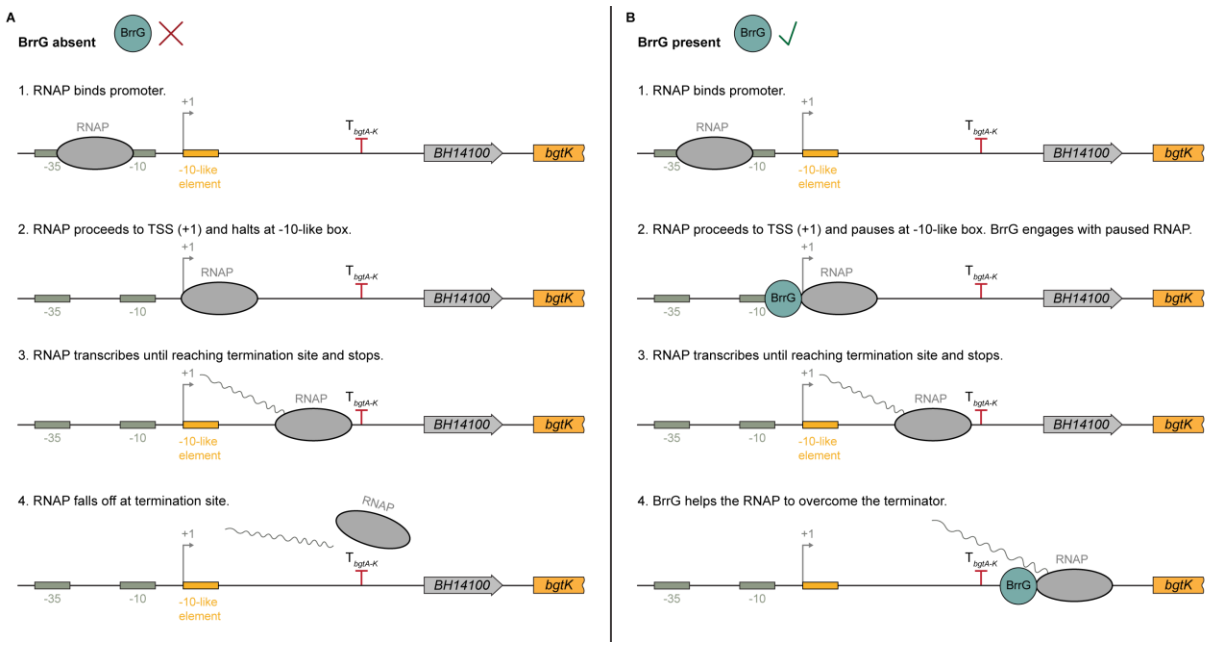


**Figure 6. Model of BrrG-antitermination. (A)** Schematic representation of terminator-dependent transcription inhibition. RNAP initiates transcription at the TSS (+1) and proceeds until the termination site ($T_{bgtA-K}$), where it falls off. **(B)** Transcriptional antitermination of the BaGTA in presence of BrrG. BrrG acts as antiterminator enabling the transcription of the downstream *bgtA-K* cassette.

285 However, why does GTA-mediated DNA transfer remain unaffected upon *brrG*
286 overexpression?

287 A simple explanation could be that bacterial lysis and particle release are controlled
288 independently of BrrG which activates only transcription of the *bgtA-K* locus. This notion is
289 supported by the apparent absence of lysis of fluorescent bacteria upon BrrG overproduction
290 (Fig. 1D). For the archetypical RcGTA of *Rhodobacter capsulatus*, particle synthesis and
291 release are controlled differentially by the CckA-ChpT-CtrA phosphorelay system, where the
292 phosphorylation state of CtrA controls the progression from the GTA synthesis to a lytic release
293 (Farrera-Calderon et al., 2021; Fogg, 2019; Westbye et al., 2018; Westbye et al., 2013). We
294 hypothesize that similarly to RcGTA a trigger could be involved in the regulation of bacterial lysis
295 and BaGTA release. BaGTA contains two putative lysis cassettes – *bgtAB* and *bgtTUV* – and

296 only the former one is located within the larger *bgt* cluster, suggesting that the latter cassette is
297 controlled independently.

298 Taken together, we demonstrate that the transcriptional control mechanism involving
299 transcription attenuation and antitermination, as described for phage lambda, is functionally
300 conserved in the chimeric BaGTA. This mechanism specifically coordinates the temporal
301 expression of the ROR and *bgtA-K* loci, which have independent phage origins. The ROR-
302 encoded BrrG acts as a processive antiterminator, facilitating the induction of the *bgtA-K*
303 transcriptional unit. However, is this regulatory mechanism also conserved in other types of GTA
304 beyond BaGTA of *Bartonella*? The recent publication by Tran and Le has shown that
305 termination-antitermination is involved in control of gene expression in evolutionary distinct
306 CcGTA of *Caulobacter crescentus* (Tran and Le, 2024). The authors showed that transcription
307 of the structural genes, which are counterparts of the *bgtA-K* locus, is co-activated by GafY and
308 IHF, while the GafZ antiterminator prevents expression attenuation at the termination sites.
309 Furthermore, GafYZ regulators of CcGTA are homologous to N'- and C'-domains of the highly
310 conserved GafA – the direct activator of RcGTA (Fogg, 2019; Gozzi et al., 2022; Sherlock and
311 Fogg, 2022), which indicates that RcGTA might also be controlled by processive antitermination.
312 Previous studies of GafA indicated that its C'-domain has similarity to the region 4 of a sigma
313 factor (R4σ) and therefore authors proposed GafA as an alternative sigma factor or a
314 transcription factor (Fogg, 2019; Sherlock and Fogg, 2022). However, the related R4σ-like fold
315 was also found in the resolved structure of Q21 antiterminator indicating that findings of Fogg
316 and Sherlock might, in fact, speak for the implication of GafA in antitermination (Shi et al.,
317 2019). Interestingly, Tran and Le found neither sequence nor structural similarity of GafZ to
318 known antiterminators Qλ and Q21. Our comparison of resolved structure of Q21 and modelled
319 BrrG, GafZ and GafA, clearly indicates similar structural features, suggesting both GafZ and
320 GafA being antiterminators (Suppl. Figure 1).

321 RcGTA and CcGTA , on one hand, and BaGTA on the other, belong to two evolutionary
322 distinct groups of GTA that emerged from independent events of phage domestication (Kogay et
323 al., 2022; Tamarit et al., 2018). The reliance of these groups on the termination-antitermination

mechanism of transcription control clearly suggests that processive antitermination is a common regulatory mechanism in GTAs, which evolved independently in two types of GTA within Alphaproteobacteria. To date, five types of GTAs have been identified in both bacteria and archaea. Given their phage heritage, it remains unclear whether other GTA types also depend on processive antitermination for regulation, and this should be explored in future studies.

330 **Materials and Methods**

331 **Bacterial Strains and growth conditions**

332 All bacterial strains, plasmids and oligonucleotides used in this study are listed in
333 Supplementary Tables 1, 2 and 3, respectively. *B. henselae* strains were grown at 35°C on
334 Columbia blood agar (CBA) supplemented with 5% sheep blood, appropriate antibiotics
335 (gentamicin (Gm) – 10 µg/ml, kanamycin (Km) – 30 µg/ml, streptomycin (Sm) – 100 µg/ml,
336 spectinomycin (Sp) – 50 µg/ml) and other supplements (isopropyl β-D-thiogalactosidase (IPTG)
337 – 500 µM, anhydrotetracycline (aTc) – 10 ng/ml or 25 ng/ml) in a humidified atmosphere
338 containing 5% $CO_2$. *B. henselae* strains were stored as cryostocks at -80°C and prior the
339 experiment seeded on CBA for 3 days and subsequently expanded and grown on fresh plates
340 for 2 days. *E. coli* strains were stored as cryostocks at -80°C and were grown at 37°C overnight
341 in lysogeny broth (LB) or on solid LB agar plates (LA) supplemented with appropriate antibiotics
342 (ampicillin (Ap) – 100 µg/ml, Gm – 10 µg/ml, Km – 30 µg/ml) and other supplements (2,6-
343 diaminopimelic acid (DAP) – 1 mM, 1% glucose).

344 **Construction of strains**

345 All bacterial strains used in this study are listed in Table 1.
346 DNA manipulations were performed according to standard techniques and all cloned inserts
347 were DNA sequenced to confirm sequence integrity. Chromosomal insertions or deletions in *B.*
348 *henselae* were generated by a two-step gene replacement procedure as described in Schulein
349 and Dehio (Schulein and Dehio, 2002). Plasmids were introduced into *B. henselae* strains by
350 conjugation with *E. coli* strain JKE201 (MFD*pir*) using two-parental mating as described
351 previously (Harms et al., 2017).

352 **Construction of plasmids**

353 All plasmids used in this study are listed in Table 2 and all oligonucleotides used in this study
354 are listed in Table 3. Plasmids generated in this study were constructed as follows:
355 pQN011: Plasmid pTR1000 was digested with the restriction enzyme BamHI.
356 Homologous fragments 1 (upstream) and 2 (downstream) were PCR amplified from heat-killed

357 *B. henselae* cells with primers prQN029 and prQN030, prQN031 and prQN032, respectively.
358 Those two fragments were cloned together by performing overlap extension PCR with primers
359 prQN030 and prQN032. The fragment and the backbone were fused with the 5X In-Fusion® HD
360 Enzyme Premix kit.

361 pQN018: *brrG* was PCR amplified from heat-killed *B. henselae* cells with primers
362 prQN053 and prQN054. *tetR* was PCR amplified with primer prAK227 and prAK208 from 705-
363 bp *tetR*-$P_{tet}$ promoter template ordered as a synthetic fragment from Genescript. The PCR
364 product generated by amplifying pBZ485_a_empty with prAK089 and prAK109 was used as a
365 backbone. Three fragments were combined with the 5X In-Fusion® HD Enzyme Premix kit.

366 pAK126: *brrG* was PCR amplified from heat-killed *B. henselae* cells with primers
367 prAK440 and prAK441. *tetR* was PCR amplified with primer prAK444 and prAK208 from 705-bp
368 *tetR*-$P_{tet}$ promoter template ordered as a synthetic fragment from Genescript. The PCR product
369 generated by amplification of pPG100 with prAK116 and prAK167 was used as a backbone.
370 Three fragments were combined with the 5X In-Fusion® HD Enzyme Premix kit.

371 pQN003: Fragment Pf3 was PCR amplified from heat-killed *B. henselae* cells with
372 primers prQN005 and prQN014. *dsRed* was PCR amplified from pJC44 with primer prAK097
373 and prAK110. The PCR product generated by amplifying pBZ485_a_empty with prAK089 and
374 prAK109 was used as a backbone. Three fragments were combined with the 5X In-Fusion® HD
375 Enzyme Premix kit.

376 pQN006: g*fpmut2* was PCR amplified from plasmid pCD353 with primers prQN015 and
377 prQN016. The PCR product generated by amplifying pBZ485_a_empty with prAK089 and
378 prAK109 was used as a backbone. Two fragments were combined with the 5X In-Fusion® HD
379 Enzyme Premix kit.

380 pQN008: Plasmid pQN006 was digested with BamHI. Fragment sF1 was PCR amplified
381 form heat-killed *B. henselae* cells with primers prQN021 and prQN022. The fragment and the
382 backbone were ligated with the 5X In-Fusion® HD Enzyme Premix kit.

383 pQN009: Plasmid pQN006 was digested with BamHI. Fragment sF2 was PCR amplified
384 form heat-killed *B. henselae* cells with primers prQN018 and prQN017. The fragment and the
385 backbone were ligated with the 5X In-Fusion® HD Enzyme Premix kit.

386 pQN010: Plasmid pQN006 was digested with BamHI. Fragment sF3 was PCR amplified
387 form heat-killed *B. henselae* cells with primers prQN019 and prQN020. The fragment and the
388 backbone were ligated with the 5X In-Fusion® HD Enzyme Premix kit.
389 pQN020: The minimal predicted $P_{GTA}$ promoter was introduced into plasmid pQN006 by
390 PCR with the primers prQN061 and prQN062. The plasmid was circularized with the 5X In-
391 Fusion® HD Enzyme Premix kit.
392 pQN057: The PCR product generated by amplifying pQN006 with prQN111 and prAK109
393 was used as a backbone. F1 was PCR amplified from heat-killed *B. henselae* cells with primers
394 prQ134 and prQN135. F1 and the backbone were combined with the 5X In-Fusion® HD
395 Enzyme Premix kit.
396 pQN058: The PCR product generated by amplifying pQN006 with prQN111 and prAK109
397 was used as a backbone. F2 was PCR amplified from heat-killed *B. henselae* cells with primers
398 prQ134 and prQN136. F2 and the backbone were ligated with the 5X In-Fusion® HD Enzyme
399 Premix kit.
400 pQN059: The PCR product generated by amplifying pQN006 with prQN111 and prAK109
401 was used as a backbone. F3 was PCR amplified from heat-killed *B. henselae* cells with primers
402 prQ134 and prQN137. F3 and the backbone were ligated with the 5X In-Fusion® HD Enzyme
403 Premix kit.
404 pQN060: The PCR product generated by amplifying pQN006 with prQN111 and prAK109
405 was used as a backbone. F4 was PCR amplified from heat-killed *B. henselae* cells with primers
406 prQ134 and prQN138. F4 and the backbone were ligated with the 5X In-Fusion® HD Enzyme
407 Premix kit.
408 pQN061: The PCR product generated by amplifying pQN006 with prQN111 and prAK109
409 was used as a backbone. F5 was PCR amplified from heat-killed *B. henselae* cells with primers
410 prQ134 and prQN139. F5 and the backbone were ligated with the 5X In-Fusion® HD Enzyme
411 Premix kit.
412 pQN007: Fragment F6 was PCR amplified from heat-killed *B. henselae* cells with
413 primers prQN005 and prQN014. Plasmid pQN006 and F6 were restricted with BamHI and Xmal
414 and ligated with RAPID DNA Dephos and Ligation Kit.

415 pQN047: The mutated -10-like sequence was introduced into plasmid pQN007 by PCR
416 with primers prQN120 and prQN121. The plasmid was circularized with the 5X In-Fusion® HD
417 Enzyme Premix kit.
418 pQN048: N'-3x-FLAG was introduced into pQN018 by PCR with primers prQN114 and
419 prQN115. The plasmid was circularized with the 5X In-Fusion® HD Enzyme Premix kit.
420 pQN049: C'-3x-FLAG was introduced into pQN018 by PCR with primers prQN116 and
421 prQN117. The plasmid was circularized with the 5X In-Fusion® HD Enzyme Premix kit.
422 pAK180: Terminator $T_{BBa_1006}$ was introduced into pQN058 by PCR with primers prAK592
423 and prAK593. The linear PCR product was used for the direct transformation of *E. coli.*
424

425 **Measuring expression of the BaGTA locus with flow cytometry**

426 *B. henselae* strains were grown as described above. Bacteria were resuspended in M199
427 supplemented with 10% FCS and other additives, e.g. inducer, if required (hereafter M199+),
428 diluted to $OD_{600\ nm}$ = 0.008 and incubated in 24-well plate for a defined amount of time in a
429 humidified atmosphere at 35°C and 5% $CO_2$. After a defined amount of time bacteria were
430 collected, centrifuged, and washed once with PBS. Bacteria were resuspended in 4% PFA and
431 fixed for 7 min at RT. The fixation was stopped by adding PBS supplemented with 2% FCS.
432 Samples were kept at 4°C in the dark before flow cytometry analysis. GFP fluorescence in
433 samples was recorded with the BD LSRFortessa™ Cell Analyzer at the FACS Core Facility,
434 Biozentrum, the University of Basel. Data were analysed using software FlowJo (Version
435 10.8.1). Visualisation of the data was done with GraphPad prism 8.

436 **GTA transfer assay**

437 GTA transfer assays were done as co-cultivations of two *B. henselae* strains. *B. henselae*
438 strains were grown as described above. Bacteria were resuspended in M199+ supplemented, if
439 required, with inducer at specified concentrations and diluted to $OD_{600\ nm}$ = 0.008. For tested co-
440 cultivation pair 1 ml of each strain was mixed and a mixture was incubated in 24-well plate for
441 24 h in a humidified atmosphere at 35°C and 5% $CO_2$. After 24 h bacteria were collected and
442 centrifuged. Bacterial pellets were resuspended in 30 µl of M199+ and resuspensions were

443 used for serial dilutions followed by plating onto CBA plates supplemented with SmGm or
444 SmGmSp antibiotics. Bacteria were grown for 6-15 d in a humidified atmosphere at 35°C and
445 5% $CO_2$. Bacterial colonies were counted, and CFU/ml was determined for each co-cultivation
446 pair. Frequency of double resistant bacteria (DRB) was calculated as the ratio of CFUs of
447 recipient DRB ($Sm^R$ $Gm^R$ $Sp^R$) / total number of recipients ($Sm^R$ $Gm^R$), yielding the transfer
448 frequency per recipient cell.

449 **Chromatin immunoprecipitation coupled with high throughput sequencing**

450 *B. henselae* strains were grown as described above. Bacteria were harvested from plates and
451 resuspended in 5 ml of Schneider's Insect Medium (24.5 g/l Schneider's Drosophila Powder
452 Medium Revised, 5% (wt/vol) sucrose, 0.025 M HEPES, adjusted pH 7.25) supplemented with
453 10% FCS (hereafter Schneider's Medium) (Guy et al., 2013; Riess et al., 2008). Bacteria were
454 diluted to $OD_{600\ nm}$ = 0.01 in 500 ml Schneider's Medium for each strain and grown at 35°C with
455 shaking 135 rpm for 4 d until $OD_{600\ nm}$ = 0.6-0.7. Bacteria were pelleted and pellets were
456 resuspended in 50 ml PBS. Bacteria were fixed with PFA with final concentration 1% and
457 incubated for 10 min at RT. The fixation was stopped by adding glycine to a final concentration
458 of 125 mM, and mixture was incubated for 20 min on ice. Fixed bacteria were centrifuged for 30
459 min at 4°C at 2000 x g, and bacterial pellets were frozen at -80°C. Thawed pellets were
460 resuspended in 10 ml of ChIP Buffer (1.1% Triton X-100, 1.2 mM EDTA, 16.7 mM Tris-HCl (pH
461 8.1), 167 mM NaCl, supplemented with cOmplete™Mini EDTA-free Protease Inhibitor Cocktail)
462 and cells were lysed by 4 passages with French Press. The lysate was sonicated, and DNA size
463 was checked with the 1.5% agarose gel. The lysate was centrifuged with the maximal speed
464 and supernatant was collected. A 50 µl aliquot of supernatant was taken as "Input DNA" for the
465 subsequent sequencing and data analysis. Following manufacturers' protocols, remaining
466 supernatant was immunoprecipitated ON with anti-FLAG Magnetic Agarose or anti-HA magnetic
467 beads for 3xFLAG-tagged and HA-tagged proteins, respectively. Magnetic beads/agarose were
468 immobilized and after removal of supernatant were sequentially rinsed with a panel of buffers:
469 Low Salt Wash Buffer (0.1% SDS, 1% Triton X-100, 2 mM EDTA, 20 mM Tris-HCl (pH 8.1), 150
470 mM NaCl), High Salt Wash Buffer (0.1% SDS, 1% Triton X-100, 2 mM EDTA, 20 mM Tris-HCl

471 (pH 8.1), 500 mM NaCl), LiCl Wash Buffer (250 mM LiCl, 1% NP-40, 1% deoxycholate, 1 mM
472 EDTA, 10 mM Tris-HCl (pH 8.1)), TBS Buffer (50 mM Tris-HCl, 150 mM NaCl). The thawed
473 Input control and immobilized Magnetic beads/agarose were mixed with 450 µl of TBS buffer, 15
474 µl of 5 M NaCl and 0.5 µl RNAse A (100mg/ml). The mixtures were incubated at 65°C ON. Then
475 4 µl of 0.5 M EDTA and 2 µl of 10 mg/ml Proteinase-K were added and the mixtures were
476 incubated at 45°C for 2 h. The resulting mixtures were thoroughly mixed in 1:1 ratio with
477 phenol/chlorophorm/isoamylalcohol combination and centrifuged at >10 000 x g for 1 min. The
478 upper aqueous phase was transferred to a new tube, mixed in 1:1 ratio with chloroform and
479 centrifuged at >10'000 x g for 1 min. The upper aqueous phase was transferred to a new tube
480 and mixed with: (i) 25 µg of linear polyacrylamide; (ii) NaAc to a final concentration of 0.3 M; (iii)
481 in 1:1 ratio with 100% isopropanol. The solution was centrifuged at >10’000 x g for 30 min,
482 washed twice with cold 70% EtOH. Pelleted DNA was dried and resuspended in water ON.
483 Library preparation and sequencing were done at the Genomics Facility Basel, D-BSSE, ETH-
484 Zurich.

485 **Bioinformatics analysis**

486 All alignments were done with the Clustal Omega and MUSCLE implemented in Geneious
487 Prime 2020.2.3 (Edgar, 2004; Sievers et al., 2011). Mapping of ChIP-Seq data was done with
488 bowtie2 (Langmead and Salzberg, 2012). Converting SAM to BAM, extracting unique binding
489 reads and sorting were done with SAMtools (Danecek et al., 2021). Coverage plots were
490 generated with bamCoverage and visualized with the Integrative Genomics Viewer (Ramírez et
491 al., 2016; Robinson et al., 2011). Promoter predictions were done with BProm (Solovyev et al.,
492 2011). Models of protein structures were either done with AlphaFold2 or taken from AlphaFold
493 Protein Structure Database (Jumper et al., 2021; Varadi et al., 2022). Comparing the predicted
494 models to Protein Data Bank (PDB) was done with the Dali server (Holm, 2022). Predictions of
495 the secondary structure of the putative terminator was done with Mfold with the default
496 parameters (Zuker, 2003). Calculations were performed at sciCORE (http://scicore.unibas.ch/)
497 scientific computing centre at the University of Basel.

498

## References


1. C. L. Turnbough. Regulation of Bacterial Gene Expression by Transcription Attenuation. *Microbiology and Molecular Biology Reviews : MMBR* **83**, e00019-00019 (2019).
2. T. J. Santangelo, I. Artsimovitch. Termination and antitermination: RNA polymerase runs a stop sign. *Nature Reviews Microbiology* **9**, 319-329 (2011).
3. J. R. Goodson, W. C. Winkler. Processive Antitermination. *Microbiology Spectrum* **6**, 6.5.05 (2018).
4. M. Québatte, C. Dehio. *Bartonella* gene transfer agent: Evolution, function, and proposed role in host adaptation. *Cellular Microbiology* **21**, e13068 (2019).
5. E. J. Banks, B. K. L. Tung. Co-opting bacterial viruses for DNA exchange: structure and regulation of gene transfer agents. *Current Opinion in Microbiology* **78** (2024).
6. M. W. Craske, J. S. Wilson, P. C. M. Fogg. Gene transfer agents: structural and functional properties of domesticated viruses. *Trends in Microbiology* 10.1016/j.tim.2024.05.002 (2024).
7. R. Kogay, S. Koppenhöfer, J. T. Beatty, J. H. Kuhn, A. S. Lang, O. Zhaxybayeva. Formal recognition and classification of gene transfer agents as viriforms. *Virus Evolution* **8**, veac100 (2022).
8. A. S. Lang, O. Zhaxybayeva, J. T. Beatty. Gene transfer agents: phage-like elements of genetic exchange. *Nature Reviews Microbiology* **10**, 472-482 (2012).
9. B. J. Arnold, I.-T. Huang, W. P. Hanage. Horizontal gene transfer and adaptive evolution in bacteria. *Nature Reviews Microbiology* **20**, 206-218 (2022).
10. E. C. Berglund, A. C. Frank, A. Calteau, O. V. Pettersson, F. Granberg, A.-S. Eriksson, K. Näslund, M. Holmberg, H. Lindroos, S. G. E. Andersson. Run-Off Replication of Host-Adaptability Genes Is Associated with Gene Transfer Agents in the Genome of Mouse-Infecting *Bartonella* grahamii. *PLOS Genetics* **5**, e1000546 (2009).
11. L. Guy, B. Nystedt, C. Toft, K. Zaremba-Niedzwiedzka, E. C. Berglund, F. Granberg, K. Näslund, A.-S. Eriksson, S. G. E. Andersson. A Gene Transfer Agent and a Dynamic

Repertoire of Secretion Systems Hold the Keys to the Explosive Radiation of the Emerging Pathogen *Bartonella*. *PLoS Genetics* **9**, e1003393 (2013).

12. M. Québatte, M. Christen, A. Harms, J. Körner, B. Christen, C. Dehio. Gene Transfer Agent Promotes Evolvability within the Fittest Subpopulation of a Bacterial Pathogen. *Cell Systems* **4**, 611-621.e616 (2017).

13. D. Tamarit, M.-M. Neuvonen, P. Engel, L. Guy, S. G. E. Andersson. Origin and Evolution of the *Bartonella* Gene Transfer Agent. *Molecular Biology and Evolution* **35**, 451-464 (2018).

14. P. Engel, W. Salzburger, M. Liesch, C.-C. Chang, S. Maruyama, C. Lanz, A. Calteau, A. Lajus, C. Médigue, S. C. Schuster, C. Dehio. Parallel Evolution of a Type IV Secretion System in Radiating Lineages of the Host-Restricted Bacterial Pathogen *Bartonella*. *PLOS Genetics* **7**, e1001296 (2011).

15. L. K. Siewert, A. Korotaev, J. Sedzicki, K. Fromm, D. D. Pinschewer, C. Dehio. Identification of the *Bartonella* autotransporter CFA as a protective antigen and hypervariable target of neutralizing antibodies in mice. *Proc Natl Acad Sci U S A* **119**, e2202059119 (2022).

16. H. C. Guo, M. Kainz, J. W. Roberts. Characterization of the late-gene regulatory region of phage 21. *Journal of Bacteriology* **173**, 1554-1560 (1991).

17. E. J. Grayhack, J. W. Roberts. The phage λ Q gene product: Activity of a transcription antiterminator in vitro. *Cell* **30** (1982).

18. Z. Yin, J. T. Kaelber, R. H. Ebright. Structural basis of Q-dependent antitermination. *Proceedings of the National Academy of Sciences* **116**, 18384-18390 (2019).

19. J. Shi, X. Gao, T. Tian, Z. Yu, B. Gao, A. Wen, L. You, S. Chang, X. Zhang, Y. Zhang, Y. Feng. Structural basis of Q-dependent transcription antitermination. *Nature Communications* **10**, 2925 (2019).

20. Z. Yin, J. G. Bird, J. T. Kaelber, B. E. Nickels, R. H. Ebright. In transcription antitermination by Qλ, NusA induces refolding of Qλ to form a nozzle that extends the RNA polymerase RNA-exit channel. *Proceedings of the National Academy of Sciences of the United States of America* **119** (2022).

555 21. E. A. Campbell, O. Muzzin, M. Chlenov, J. L. Sun, C. A. Olson, O. Weinman, M. L.
556 Trester-Zedlitz, S. A. Darst. Structure of the bacterial RNA polymerase promoter
557 specificity sigma subunit. *Mol Cell* **9**, 527-539 (2002).
558 22. K. S. Murakami, S. Masuda, E. A. Campbell, O. Muzzin, S. A. Darst. Structural basis of
559 transcription initiation: an RNA polymerase holoenzyme-DNA complex. *Science* **296**,
560 1285-1290 (2002).
561 23. S. A. Perdue, J. W. Roberts. σ70-dependent Transcription Pausing in *Escherichia coli*.
562 *Journal of Molecular Biology* **412**, 782-792 (2011).
563 24. S. R. Casjens, R. W. Hendrix. Bacteriophage lambda: Early pioneer and still relevant.
564 *Virology* **479-480**, 310-330 (2015).
565 25. R. G. Farrera-Calderon, P. Pallegar, A. B. Westbye, C. Wiesmann, A. S. Lang, J. T.
566 Beatty. The CckA-ChpT-CtrA Phosphorelay Controlling *Rhodobacter capsulatus* Gene
567 Transfer Agent Production Is Bidirectional and Regulated by Cyclic di-GMP. *Journal of*
568 *Bacteriology* **203**, e00525-00520 (2021).
569 26. P. C. M. Fogg. Identification and characterization of a direct activator of a gene transfer
570 agent. *Nature Communications* **10**, 595 (2019).
571 27. A. B. Westbye, L. Kater, C. Wiesmann, H. Ding, C. K. Yip, J. T. Beatty. The Protease
572 ClpXP and the PAS Domain Protein DivL Regulate CtrA and Gene Transfer Agent
573 Production in *Rhodobacter capsulatus*. *Applied and Environmental Microbiology* **84**,
574 e00275-00218 (2018).
575 28. A. B. Westbye, M. M. Leung, S. M. Florizone, T. A. Taylor, J. A. Johnson, P. C. Fogg, J. T.
576 Beatty. Phosphate concentration and the putative sensor kinase protein CckA modulate
577 cell lysis and release of the *Rhodobacter capsulatus* gene transfer agent. *Journal of*
578 *Bacteriology* **195**, 5025-5040 (2013).
579 29. N. T. Tran, T. B. K. Le. Control of a gene transfer agent cluster in *Caulobacter crescentus*
580 by transcriptional activation and anti-termination. *Nature Communications 2024 15:1* **15**
581 (2024).

30. K. Gozzi, N. T. Tran, J. W. Modell, T. B. K. Le, M. T. Laub. Prophage-like gene transfer agents promote *Caulobacter crescentus* survival and DNA repair during stationary phase. *PLOS Biology* **20**, e3001790 (2022).

31. D. Sherlock, P. C. M. Fogg. The archetypal gene transfer agent RcGTA is regulated via direct interaction with the enigmatic RNA polymerase omega subunit. *Cell Reports* **40**, 111183 (2022).

32. R. Schulein, C. Dehio. The VirB/VirD4 type IV secretion system of *Bartonella* is essential for establishing intraerythrocytic infection. *Molecular Microbiology* **46**, 1053-1067 (2002).

33. A. Harms, M. Liesch, J. Körner, M. Québatte, P. Engel, C. Dehio. A bacterial toxin-antitoxin module is the origin of inter-bacterial and inter-kingdom effectors of *Bartonella*. *PLOS Genetics* **13**, e1007077 (2017).

34. T. Riess, F. Dietrich, K. V. Schmidt, P. O. Kaiser, H. Schwarz, A. Schäfer, V. A. J. Kempf. Analysis of a Novel Insect Cell Culture Medium-Based Growth Medium for *Bartonella* Species. *Applied and Environmental Microbiology* **74**, 5224-5227 (2008).

35. R. C. Edgar. MUSCLE: multiple sequence alignment with high accuracy and high throughput. *Nucleic Acids Research* **32**, 1792-1797 (2004).

36. F. Sievers, A. Wilm, D. Dineen, T. J. Gibson, K. Karplus, W. Li, R. Lopez, H. McWilliam, M. Remmert, J. Söding, J. D. Thompson, D. G. Higgins. Fast, scalable generation of high-quality protein multiple sequence alignments using Clustal Omega. *Molecular Systems Biology* **7**, 539 (2011).

37. B. Langmead, S. L. Salzberg. Fast gapped-read alignment with Bowtie 2. *Nature Methods* **9**, 357-359 (2012).

38. P. Danecek, J. K. Bonfield, J. Liddle, J. Marshall, V. Ohan, M. O. Pollard, A. Whitwham, T. Keane, S. A. McCarthy, R. M. Davies, H. Li. Twelve years of SAMtools and BCFtools. *GigaScience* **10**, giab008 (2021).

39. F. Ramírez, D. P. Ryan, B. Grüning, V. Bhardwaj, F. Kilpert, A. S. Richter, S. Heyne, F. Dündar, T. Manke. deepTools2: a next generation web server for deep-sequencing data analysis. *Nucleic Acids Research* **44**, W160-W165 (2016).

40. J. T. Robinson, H. Thorvaldsdóttir, W. Winckler, M. Guttman, E. S. Lander, G. Getz, J. P. Mesirov. Integrative genomics viewer. *Nature Biotechnology* **29**, 24-26 (2011).

41. V. Solovyev, A. Salamov, I. Seledtsov, D. Vorobyev, A. Bachinsky, *Automatic Annotation of Bacterial Community Sequences and Application to Infections Diagnostic.* (2011), pp. 346.

42. J. Jumper, R. Evans, A. Pritzel, T. Green, M. Figurnov, O. Ronneberger, K. Tunyasuvunakool, R. Bates, A. Žídek, A. Potapenko, A. Bridgland, C. Meyer, S. A. A. Kohl, A. J. Ballard, A. Cowie, B. Romera-Paredes, S. Nikolov, R. Jain, J. Adler, T. Back, S. Petersen, D. Reiman, E. Clancy, M. Zielinski, M. Steinegger, M. Pacholska, T. Berghammer, S. Bodenstein, D. Silver, O. Vinyals, A. W. Senior, K. Kavukcuoglu, P. Kohli, D. Hassabis. Highly accurate protein structure prediction with AlphaFold. *Nature* **596**, 583-589 (2021).

43. M. Varadi, S. Anyango, M. Deshpande, S. Nair, C. Natassia, G. Yordanova, D. Yuan, O. Stroe, G. Wood, A. Laydon, A. Žídek, T. Green, K. Tunyasuvunakool, S. Petersen, J. Jumper, E. Clancy, R. Green, A. Vora, M. Lutfi, M. Figurnov, A. Cowie, N. Hobbs, P. Kohli, G. Kleywegt, E. Birney, D. Hassabis, S. Velankar. AlphaFold Protein Structure Database: massively expanding the structural coverage of protein-sequence space with high-accuracy models. *Nucleic Acids Research* **50**, D439-D444 (2022).

44. L. Holm. Dali server: structural unification of protein families. *Nucleic Acids Research* **50**, W210-W215 (2022).

45. M. Zuker. Mfold web server for nucleic acid folding and hybridization prediction. *Nucleic Acids Research* **31**, 3406-3415 (2003).

46. M. C. Schmid, R. Schulein, M. Dehio, G. Denecker, I. Carena, C. Dehio. The VirB type IV secretion system of *Bartonella henselae* mediates invasion, proinflammatory activation and antiapoptotic protection of endothelial cells. *Molecular Microbiology* **52**, 81-92 (2004).

47. R. Schulein, P. Guye, T. A. Rhomberg, M. C. Schmid, G. Schröder, A. C. Vergunst, I. Carena, C. Dehio. A bipartite signal mediates the transfer of type IV secretion substrates

638 of *Bartonella henselae* into human cells. *Proceedings of the National Academy of*
639 *Sciences of the United States of America* **102**, 856-861 (2005).
640 48. S. Marlaire, C. Dehio. *Bartonella* effector protein C mediates actin stress fiber formation
641 via recruitment of GEF-H1 to the plasma membrane. *PLOS Pathogens* **17**, e1008548
642 (2021).
643 49. T. Starr, T. W. Ng, T. D. Wehrly, L. A. Knodler, J. Celli. *Brucella* Intracellular Replication
644 Requires Trafficking Through the Late Endosomal/Lysosomal Compartment. *Traffic* **9**,
645 678-694 (2008).
646 50. M. Dehio, A. Knorre, C. Lanz, C. Dehio. Construction of versatile high-level expression
647 vectors for *Bartonella henselae* and the use of green fluorescent protein as a new
648 expression marker. *Gene* **215**, 223-229 (1998).

649

650

651 **Tables**

**Table 1. List of strains used in this study.**

| Strain | Plasmid | Background | Description | Reference |
|---|---|---|---|---|
| *E. coli* | | | | |
| Novablue | | | *endA1 hsdR17 (rK12– mK12+) supE44 thi-1 recA1 gyrA96 relA1 lac F'[proA+B+ lacIqZΔM15::Tn10]* | Novagen |
| HST08 | | | *F-, endA1, supE44, thi-1, recA1, relA1, gyrA96, phoA, Φ80d lacZΔ M15, Δ (lacZYA - argF) U169, Δ (mrr - hsdRMS - mcrBC), ΔmcrA, λ-* | Takara |
| JKE201 | | | *MFDpir ΔmcrA Δ(mrr-hsdRMS-mcrBC) aac(3)IV::lacIq* | (Harms et al., 2017) |
| *B. henselae* Houston-I ATCC 49882T | | | | |
| RSE247 | | | *Bartonella henselae* ATCC 49882T *$Sm^R$* | (Schmid et al., 2004) |
| AKB144 | | | Wild-type, copy of RSE247 | This work |
| MQB1366 | | | *bgtC-gfpmut2 rpsL $Sm^R$* | (Québatte et al., 2017) |
| AKB142 | | | Copy of MQB1366 *(bgtC-gfpmut2 rpsL $Sm^R$)* | This study |
| AKB229 | | AKB142 | *BH01490::Himar1($Gm^R$) bgtC-gfpmut2 rpsL $Sm^R$* | This study |
| MQB1028 | | | *ΔbgtCD -$P_{virB}$-gfp rpsL $Sm^R$* | (Québatte et al., 2017) |
| MQB1528 | pAH184 | MQB1028 | *ΔbgtCD -$P_{virB}$-gfp rpsL $Sm^R$* | This study |
| MQB759 | | | *ΔbgtCD rpsL $Sm^R$* | (Québatte et al., 2017) |
| MQB1405 | | MQB759 | *ΔbgtCD BH14050-gfpmut2 rpsL $Sm^R$* | This study |
| AKB230 | | MQB1405 | *ΔbgtCD BH_RS00695::Himar1 ($Gm^R$) BH14050-gfpmut2 rpsL $Sm^R$* | This study |
| QNB135 | | AKB229 | *ΔbrrG BH01490::Himar1 ($Gm^R$) bgtC-gfpmut2 rpsL $Sm^R$* | This study |
| QNB205 | pQN018 | QNB135 | *ΔbrrG, BH01490::Himar1 ($Gm^R$) bgtC-gfpmut2 rpsL $Sm^R$* | This study |
| QNB199 | pQN018 | AKB229 | *BH01490::Himar1 ($Gm^R$) bgtC-gfpmut2 rpsL $Sm^R$* | This study |
| AKB456 | pAK126 | AKB142 | *bgtC-gfpmut2 rpsL $Sm^R$* | This study |
| AKB411 | pQN003 | AKB144 | *rpsL $Sm^R$* | This study |
| QNB119 | pQN008 | AKB144 | *rpsL $Sm^R$* | This study |
| QNB121 | pQN009 | AKB144 | *rpsL $Sm^R$* | This study |
| QNB123 | pQN010 | AKB144 | *rpsL $Sm^R$* | This study |
| QNB159 | pQN020 | AKB144 | *rpsL $Sm^R$* | This study |
| QNB194 | pQN057 | AKB144 | *rpsL $Sm^R$* | This study |
| QNB195 | pQN058 | AKB144 | *rpsL $Sm^R$* | This study |
| QNB196 | pQN059 | AKB144 | *rpsL $Sm^R$* | This study |
| QNB197 | pQN060 | AKB144 | *rpsL $Sm^R$* | This study |
| QNB198 | pQN061 | AKB144 | *rpsL $Sm^R$* | This study |
| AKB460 | pQN007 | AKB144 | *rpsL $Sm^R$* | This study |
| QNB176 | pQN047, pAK126 | AKB144 | *rpsL $Sm^R$* | This study |
| AKB461 | pQN007, pAK126 | AKB144 | *rpsL $Sm^R$* | This study |
| QNB185 | pQN048 | QNB135 | *ΔbrrG BH01490::Himar1($Gm^R$) bgtC-gfpmut2 rpsL $Sm^R$* | This study |
| QNB186 | pQN049 | QNB135 | *ΔbrrG BH01490::Himar1($Gm^R$) bgtC-gfpmut2 rpsL $Sm^R$* | This study |
| AKB528 | pQN058, pAK126 | QNB195 | *rpsL $Sm^R$* | This study |
| AKB572 | pAK180, pAK126 | AKB144 | *rpsL $Sm^R$* | This study |

652

**Table 2. List of plasmids used in this study.**

| Plasmid | Resistance | Description | Reference |
|---|---|---|---|
| pTR1000 | *Km*$^R$ | Suicide plasmid for *Bartonella* mutagenesis | (Schulein et al., 2005) |
| pBZ485_a_empty | *Km*$^R$ | $P_{taclac}$-*none*. Empty control plasmid | (Marlaire and Dehio, 2021) |
| pMQ999-1 | *Gm*$^R$, *Amp*$^R$ | *Gm*$^R$ *Himar1* transposon plasmid | (Québatte et al., 2017) |
| pAH184 | *Sp*$^R$ | Plasmid for the GTA transfer | (Québatte et al., 2017) |
| pQN011 | *Gm*$^R$ | Deletion of *brrG* | This study |
| pQN018 | *Km*$^R$ | $P_{tet}$-*brrG*. Plasmid for *brrG* overexpression. $RSF1010_{ori}$ | This study |
| pPG100 | *Gm*$^R$ | Plasmid with pBGR1 origin | (Schulein et al., 2005) |
| pAK126 | *Gm*$^R$ | $P_{tet}$-*brrG*. Plasmid for *brrG* overexpression. | This study |
| pJC44 | *Gm*$^R$ | Plasmid with constitutively expressed *dsRed* | (Starr et al., 2008) |
| pQN003 | *Km*$^R$ | $P_{Pf3}$-*dsRed*. Promoter probe plasmid | This study |
| pCD353 | *Km*$^R$ | $P_{taclac}$-*gfpmut2*. Plasmid for *gfpmut2* overexpression | (Dehio et al., 1998) |
| pQN006 | *Km*$^R$ | $P_{none}$-*gfpmut2.* Promoter probe plasmid | This study |
| pQN008 | *Km*$^R$ | p*sF1-gfpmut2*. Promoter probe plasmid | This study |
| pQN010 | *Km*$^R$ | p*sF2-gfpmut2*. Promoter probe plasmid | This study |
| pQN009 | *Km*$^R$ | p*sF3-gfpmut2*. Promoter probe plasmid | This study |
| pQN020 | *Km*$^R$ | p*F0-gfpmut2*. Minimal predicted $P_{GTA}$ promoter | This study |
| pQN057 | *Km*$^R$ | p*F1-gfpmut2*. Plasmid with truncation of promoter region | This study |
| pQN058 | *Km*$^R$ | p*F2-gfpmut2*. Plasmid with truncation of promoter region | This study |
| pQN059 | *Km*$^R$ | p*F3-gfpmut2*. Plasmid with truncation of promoter region | This study |
| pQN060 | *Km*$^R$ | p*F4-gfpmut2*. Plasmid with truncation of promoter region | This study |
| pQN061 | *Km*$^R$ | p*F5-gfpmut2*. Plasmid with truncation of promoter region | This study |
| pQN007 | *Km*$^R$ | p*F6-gfpmut2*. Plasmid with truncation of promoter region | This study |
| pQN047 | *Km*$^R$ | pQN007 with mutated -10-like element | This study |
| pQN048 | *Km*$^R$ | $P_{tet}$-*3xFLAG-brrG*. Plasmid for BrrG immunoprecipitation | This study |
| pQN049 | *Km*$^R$ | $P_{tet}$-*brrG-3xFLAG*. Plasmid for BrrG immunoprecipitation | This study |
| pAK180 | *Km*$^R$ | p*F2-*$T_{BBa_1006}$-*gfpmut2.* Plasmid for testing BrrG antitermination properties | This study |

**Table 3. List of oligonucleotides used in this study.**

| Oligonucleotide identifier | Sequences (5' to 3') |
|---|---|
| prAK089 | GTTAAGCCTTTTCTGAGCATGG |
| prAK109 | GAAGCGGAACACGTAGAAAGC |
| prAK227 | ATGCTCAGAAAAGGCTTAACTTAAGACCCACTTTCACATTTAAG |
| prAK208 | CTTCACTTTTCTCTATCACTGATAG |
| prQN029 | CCTGACGCCCCCGGGGATCCCCCTTACATCTTACAGCACTATC |
| prQN030 | AGAGATTATTTAGAGTCTTAATGTTTCATGTCATCTCCTCAAAA |
| prQN031 | TAAGACTCTAAATAATCTCTGTG |
| prQN032 | AGGTCGACTCTAGAGGATCCCAGAGCAAAATGGACATTCAAAT |
| prQN005 | ATATATATCCCGGGAGATACTGTTCTAGAAATGAGG |
| prQN053 | AGTGATAGAGAAAAGTGAAGAAGGAGATATACAAATGAAACATCAAGATAAAAGA AAAAA |
| prQN054 | GCTTTCTACGTGTTCCGCTTCTTAACCGCTTGTATATCCCCAA |
| prAK440 | AGTGATAGAGAAAAGTGAAGAAGGAGATATACATATGAAACATCAAGATAAAAGA AAAAAC |
| prAK441 | TGCGAGAGTAGGGAACTGCCTTAACCGCTTGTATATCCCCAATG |
| prAK444 | AGTGAGCGAGGAAGCGGAAGTTAAGACCCACTTTCACATTTAAG |
| prAK116 | GGCAGTTCCCTACTCTCGC |
| prAK167 | CTATTTCATTATGGTGAAAGTTGGAACCTCTTACGTCTTCCGCTTCCTCGCTCAC TG |
| prQN014 | ATATAGGATCCCATCCTGTTCCTTCAAATTAAAGAGAAGCTGATCCC |
| prAK097 | ATGCTCAGAAAAGGCTTAACCTACTGGGAGCCGGAGTG |
| prAK110 | CTTTCTACGTGTTCCGCTTCACTGACGCGAATTCCCGGGGATCCTCTAGATTTA AGAAGGAGATATACATATGGACAACACCGAGGACG |
| prQN015 | GCTTTCTACGTGTTCCGCTTCGAATTCGTCGACCCCGGGTCTAGAGGATCCTTT AAGAAGGAGATATACATATGA |
| prQN016 | CCATGCTCAGAAAAGGCTTAACTTATTTGTATAGTTCATCCATGCC |
| prQN021 | ACCCCGGGTCTAGAGGATCCATGAGTGTAGGTCTTTCTCGT |
| prQN022 | ATCTCCTTCTTAAAGGATCCCATCCTGTTCCTTCAAATTAAAG |
| prQN017 | ACCCCGGGTCTAGAGGATCCGATACTGTTCTAGAAATGAGGA |
| prQN018 | ATCTCCTTCTTAAAGGATCCTGACAAAGTCTGACCGATGAG |
| prQN019 | ACCCCGGGTCTAGAGGATCCGTTTGTAAATCAAACACTATCTG |
| prQN020 | ATCTCCTTCTTAAAGGATCCCCGTTACAGCTTCCAACAAAG |
| prQN061 | TCCTCTAGACCCGGGGTCGAATGATACGCGTTCAGATTTACCTTGTCAATCGAC GAATTCGAAGCGGAA |
| prQN062 | TTCCGCTTCGAATTCGTCGATTGACAAGGTAAATCTGAACGCGTATCATTCGAC CCCGGGTCTAGAGGA |
| prQN111 | TCGACCCCGGGTCTAGAGG |
| prQN134 | CTTTCTACGTGTTCCGCTTCTTGACAAGGTAAATCTGAACGCG |
| prQN135 | TCCTCTAGACCCGGGGTCGAAAGCACAGAATGCTGATTGTATC |
| prQN136 | TCCTCTAGACCCGGGGTCGAAAAGCTCTAAGAAAGACAGAACC |
| prQN137 | TCCTCTAGACCCGGGGTCGATGACAAAGTCTGACCGATGAGT |
| prQN138 | TCCTCTAGACCCGGGGTCGAGGATTACCAAGAATGTATCATTATA |
| prQN139 | TCCTCTAGACCCGGGGTCGATCTCCCGTTACAGCTTCCAAC |
| prQN120 | ATGCTGGTTGCATCATTATGATACGCGTTCAGAT |
| prQN121 | CATAATGATGCAACCAGCATTCTGTGCTTTTGTGA |
| prQN114 | TTATAATCAATATCATGATCCTTATAATCACCGTCATGATCTTTATAATCCATTTGTA TATCTCCTTCTTCAC |
| prQN115 | GATCATGATATTGATTATAAAGACGACGATGACAAGGGTGGAGGTGGCTCTAAA CATCAAGATAAAAGAAAAAACAC |
| prQN116 | AATCAATATCATGATCCTTATAATCACCGTCATGATCTTTATAATCAGAGCCACCT CCACCACCGCTTGTATATCCCCAATG |
| prQN117 | TAAGGATCATGATATTGATTATAAAGACGACGATGACAAGTAAGAAGCGGAACAC GTAGAAA |
| prAK592 | GCCCTGTCAGGGGCGGGGTTTTTTTTTAAAGCTCTAAGAAAGACAGAACC |
| prAK593 | AACCCCGCCCCTGACAGGGCGGGGTTTTTTTTTCGACCCCGGGTCTAGAGG |

655

656 **Supplementary Figures:**

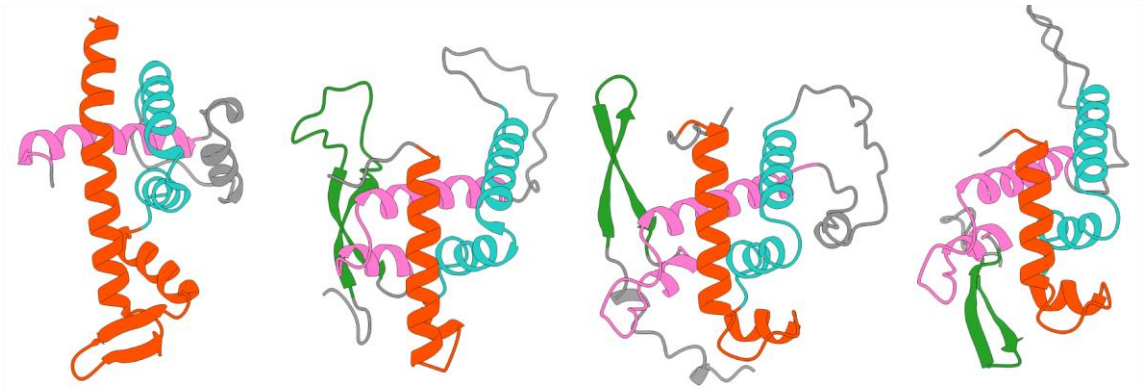

| | Q21 (6p1b) | $BrrG_{26-188}$ | $GafA_{201-382}$ | $GafZ_{89-244}$ |
|---|---|---|---|---|
| DALI Z-score | 0 | 6.7 | 7.0 | 5.7 |
| Rmsd score (Å) | 28.4 | 2.6 | 2.9 | 3.0 |
| Residue number | 150 | 163 | 182 | 156 |

**Suppl. Figure 1. BrrG, GafA and GafZ share structural features**. Structure of Q21 (6p1b) and AlphaFold2 models of BrrG (partial, A0A0R4J952), GafA (partial, D5AUH1) and GafZ (partial, A0A0H3C763). Similar features are shown in the same colour. Table below illustrates DALI Z-score and Rmsd score analysis of structural similarities. AlphaFold2 models were aligned to structure of Q21 (6p1b) using DALI Server (http://ekhidna2.biocenter.helsinki.fi/dali/). Higher Z-scores, respectively lower Rmsd values suggest better alignment and similarity to the reference structure.

657

658

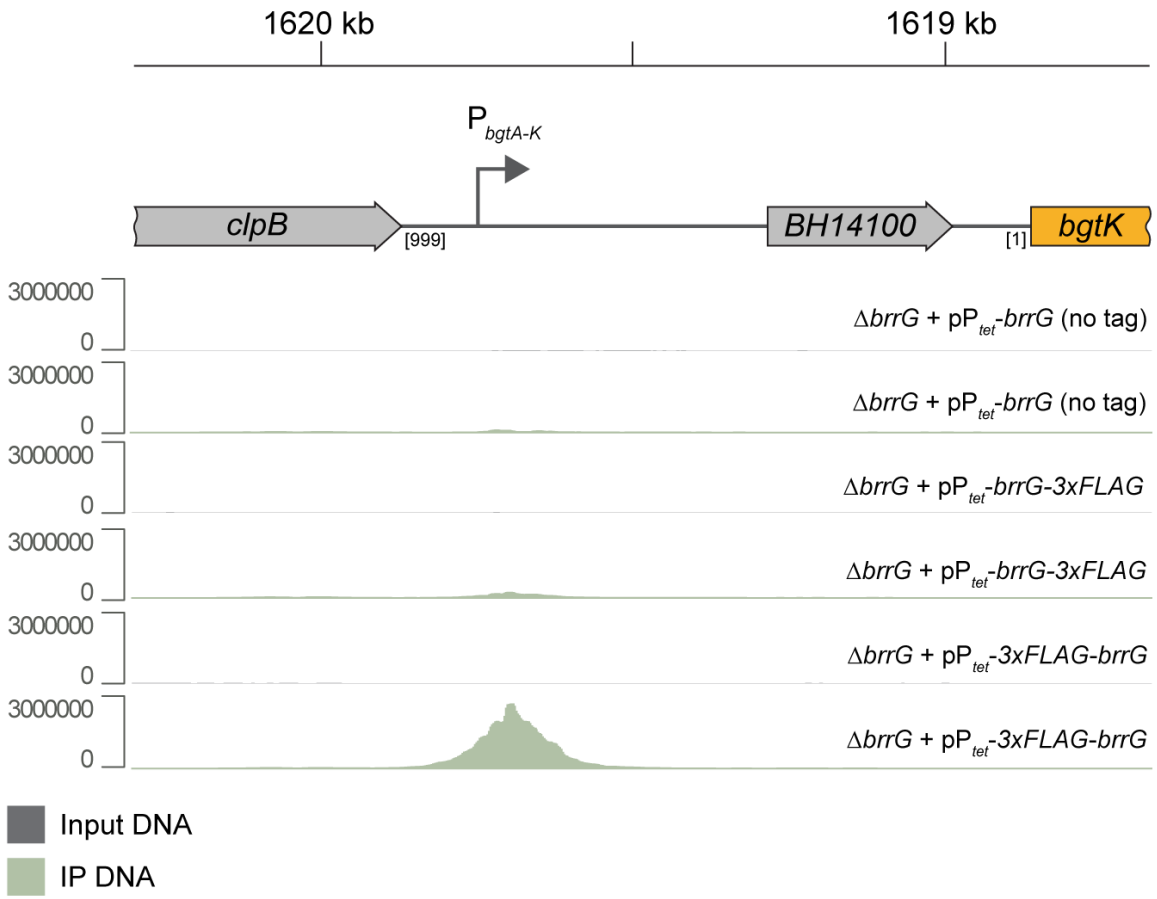


**Suppl. Figure 2. BrrG binds in the promoter region $P_{bgtA\text{-}K}$ in front of the *bgtA-K* cluster.** Location of the $P_{bgtA\text{-}K}$ promoter and of the BrrG binding site of Δ*brrG* + $pP_{tet}$-*3xFLAG-brrG*- identified by ChIP-Seq. IP DNA is shown in green and input DNA in dark grey. Δ*brrG* + $pP_{tet}$-*brrG* was used as control. One replicate per strain is shown. Scale on the left indicates the coverage of the enriched DNA. Scale on the top indicates the genomic position in the *Bartonella henselae* genome.

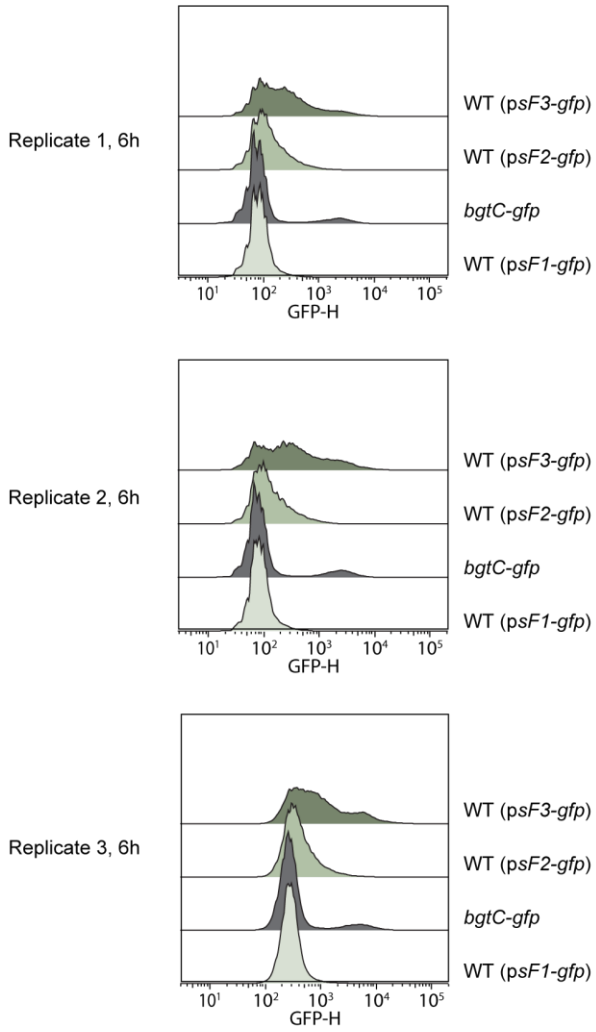


667

668 **Suppl. Figure 3. The $P_{bgtA\text{-}K}$ promoter is located far upstream of the *bgtA-K* locus.**
669 Fluorescence distribution at the 6 h time-point. Strain *bgtC-gfp* displaying wild-type expression
670 pattern of the *bgtA-K* locus was used as control**.** The time-course experiments were started with
671 the incubation of CBA agar-grown bacteria in M199 medium supplemented with 10% FCS. The
672 experiments were done in biological triplicates.

673

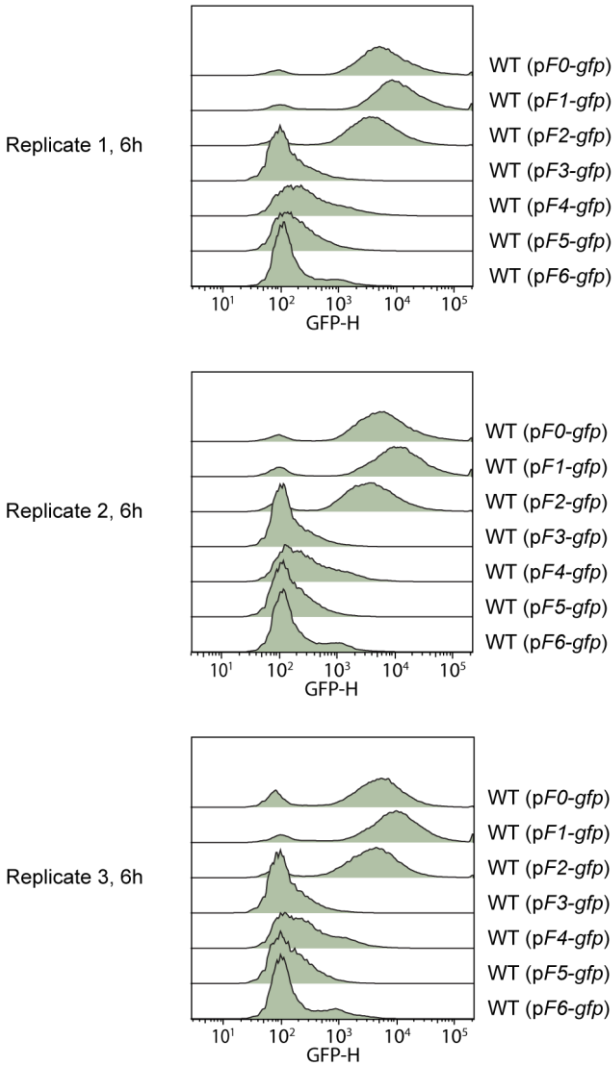


674

675 **Suppl. Figure 4. Fluorescence distribution for the bacterial populations containing the**
676 **promoter-probe plasmids with various truncations at 6 h.** The time-course experiments
677 were started with the incubation of CBA agar-grown bacteria in M199 medium supplemented
678 with 10% FCS. The experiments were done in biological triplicates.

679

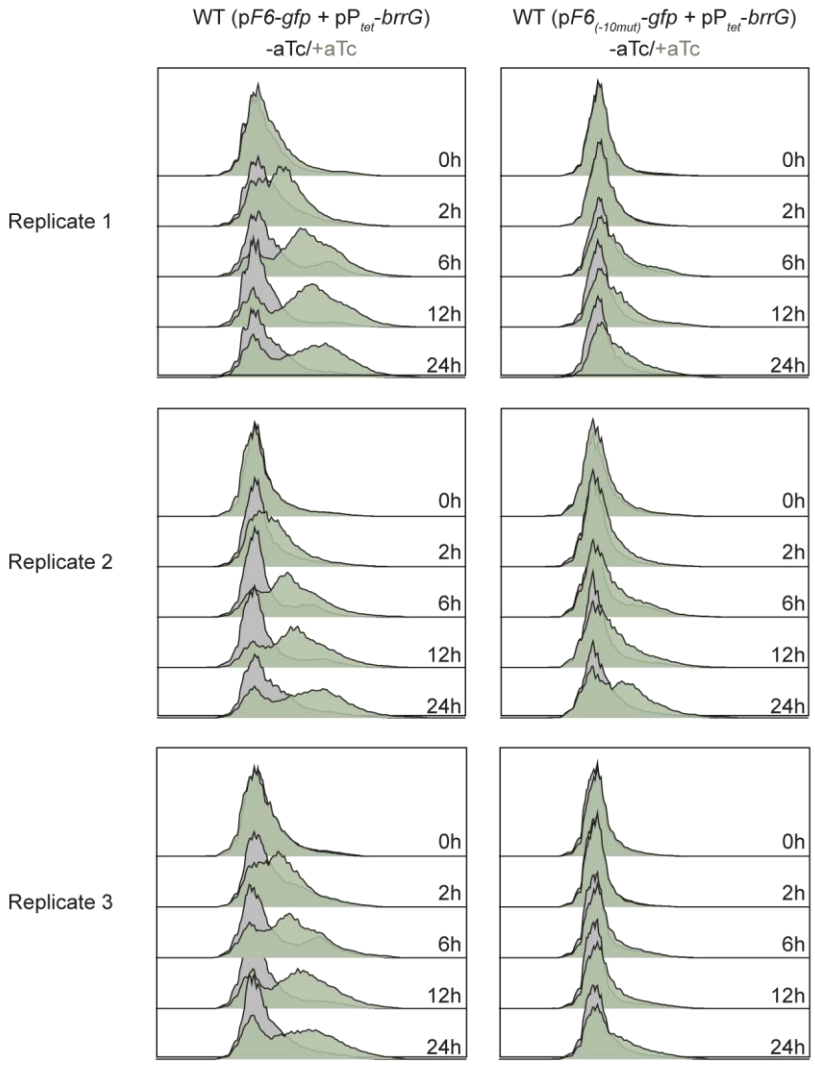


680

681 **Suppl. Figure 5. The -10-like element downstream of the P$_{bgtA-K}$ promoter is crucial for the**
682 **antitermination by BrrG.** Histograms of fluorescence distribution for the bacterial populations
683 containing the promoter-probe plasmid pF6 with the P$_{bgtA-K}$ promoter and the adjacent native -
684 10-like element or its derivative, plasmid p*F6*$_{(-10mut)}$, carrying mutations in two conserved
685 positions of the -10-like element. Plasmid pP$_{tet-brrG}$ encodes an aTc-inducible *brrG* expression
686 cassette. BrrG overproduction was induced by 25 ng/ml aTc. The time-course experiment was
687 started with the incubation of CBA plate-grown bacteria in M199 medium supplemented with
688 10% FCS. Inducer aTc was added at time-point 0 h. Experiments were performed in biological
689 triplicates.

690

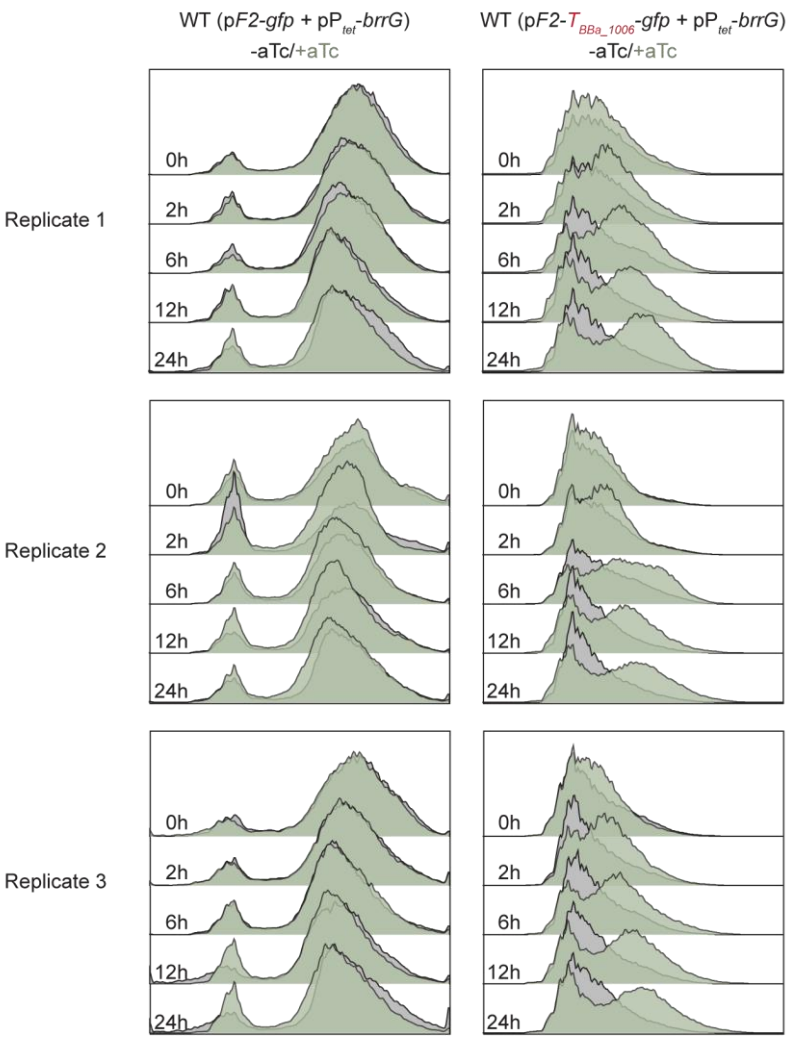


691

692 **Suppl. Figure 6. Fluorescence distribution for the bacterial populations containing the**
693 **fragment F2 (Fig. 2A), the fragment F2 with the terminator and the sequence with the**
694 **mutated -10-like element (pF6$_{-10mut}$).** Time of the measurements is indicated. Induction was
695 done with 25 ng/ml aTc. Bacteria were cultivated in M199 medium supplemented with 10% FCS
696 and aTc inducer at indicated concentrations. Experiments were performed in biological
697 triplicates.

698

**Acknowledgement**

We thank the FACS Core Facility of the Biozentrum for allowing us to conduct our FACS experiments and Dr. Jaroslaw Sedzicki for analysis for the structural analysis and figure preparation of the structure models. This work was supported by the Swiss National Science Foundation (SNSF, www.snf.ch) grant 310030B_201273 (to C.D.)